

# Stress field changes in Central Europe from Late Miocene to Quaternary as determined from volcanic rocks in the Bohemian Massif

Jakub Stemberk<sup>1</sup>, Miroslav Coubal<sup>1</sup>, and Petra Štěpančíková<sup>1</sup>

<sup>1</sup>Institute of Rock Structure and Mechanics of the Czech Academy of Sciences

November 24, 2022

## Abstract

This work presents the results of a paleostress investigation in dated Mio-Pliocene volcanic rocks in the vicinity of the town of Lądek Zdrój in the Rychlebské hory Mts., as a part of the central Sudetic Mts. in the NE Bohemian Massif. Six different paleostress field regimes from the Late Miocene to Quaternary were distinguished. Each stress regime is characterized by the orientation of the principal parameters and is discussed in relation to the known paleostress regimes within the surrounding regions of the Sudetic Mts., Fore-Sudetic block, and European Alpine foreland in Central Europe. The results show switching of tectonic phases with dominant compression, transtension or extension. Moreover, the orientation of theoretical planes with maximum shear stress and with a high tendency to dilate for individual paleostress regimes is defined and compared with the orientation of known faults within the study area suggesting their possible kinematics. The timing of the derived regimes is determined more accurately and is in good accordance with the data reported from different regions in Central Europe, which suggests their broader validity. In addition, one event or shorter events interrupting the main Plio-Quaternary extensional regime and one differently oriented Plio-Quaternary extension regime were discovered and constrained based on several dated phases of the volcanism of the faulted rocks.

# 1 Stress field changes in Central Europe from Late Miocene to Quaternary as 2 determined from volcanic rocks in the Bohemian Massif

3 J. Stemberk Jr.<sup>1,2</sup>, M. Coubal<sup>1,3</sup>, and P. Štěpančíková<sup>1</sup>

4 <sup>1</sup>Institute of Rock Structure and Mechanics, The Czech Academy of Sciences, V Holešovičkách  
5 94/41, Prague 8, 18000, Czech Republic.

6 <sup>2</sup>Faculty of Science, Charles University, Albertov 6, Prague 2, 12800, Czech Republic.

7 <sup>3</sup>Institute of Geology, The Czech Academy of Sciences, Rozvojová 269, Prague 6, 16000, Czech  
8 Republic.

9 Corresponding author: Jakub Stemberk ([jakub.stemberk@irsm.cas.cz](mailto:jakub.stemberk@irsm.cas.cz))

## 10 Key Points:

- 11 • Redefined timing of stress field changes since the Late Miocene in the W & N European  
12 Alpine foreland based on striae in dated volcanic rock
- 13 • New compressional and extensional stress regimes were discovered postdating 3.83 Ma
- 14 • Defined the behavior of the Sudetic Marginal fault and the Biala fault since Late Miocene  
15 to Quaternary

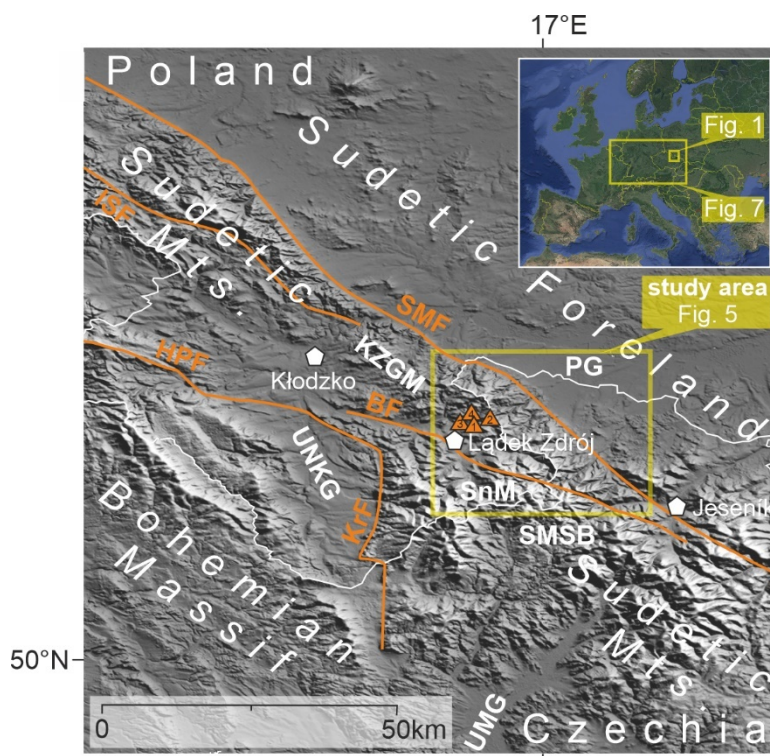
## 16 Abstract

17 This work presents the results of a paleostress investigation in dated Mio-Pliocene volcanic rocks  
18 in the vicinity of the town of Lądek Zdrój in the Rychlebské hory Mts., as a part of the central  
19 Sudetic Mts. in the NE Bohemian Massif. Six different paleostress field regimes from the Late  
20 Miocene to Quaternary were distinguished. Each stress regime is characterized by the orientation  
21 of the principal parameters and is discussed in relation to the known paleostress regimes within  
22 the surrounding regions of the Sudetic Mts., Fore-Sudetic block, and European Alpine foreland  
23 in Central Europe. The results show switching of tectonic phases with dominant compression,  
24 transtension or extension. Moreover, the orientation of theoretical planes with maximum shear  
25 stress and with a high tendency to dilate for individual paleostress regimes is defined and  
26 compared with the orientation of known faults within the study area suggesting their possible  
27 kinematics. The timing of the derived regimes is determined more accurately and is in good  
28 accordance with the data reported from different regions in Central Europe, which suggests their  
29 broader validity. In addition, one event or shorter events interrupting the main Plio-Quaternary  
30 extensional regime and one differently oriented Plio-Quaternary extension regime were  
31 discovered and constrained based on several dated phases of the volcanism of the faulted rocks.

## 32 1.1 Introduction

33 The Rychlebské hory Mts. (RH)/Złote Góry Mts. are situated in the NE part of the  
34 Bohemian Massif. They represent an aligned mountain ridge along the NW-SE striking Sudetic  
35 Marginal fault (SMF), which belongs to one of the most important faults in Central Europe  
36 (Badura et al., 2003; 2007; Ivan, 1966; Krzyszkowski et al., 1995; Oberc & Dyjor, 1969;

37 Štěpančíková et al., 2008; etc.). The SMF separates the relatively subsided Fore-Sudetic block in  
 38 the NE, with the Sudetic Foreland (Fig. 1) formed by gently undulated relief with scattered  
 39 groups of hills or slightly dissected uplands, from the elevated Sudetic block in the SW with the  
 40 mountain ranges of the Sudetic Mts. with broad ridges and deeply dissected uplands and with an  
 41 average elevation of 400-800 m a. s. l. (Štěpančíková & Stemberk Jr. 2016, Fig. 1). The Fore-  
 42 Sudetic block is covered by a sequence of Miocene-Quaternary sediments (FSB, Fig. 6). The  
 43 SMF zone was probably formed in the early Variscan and since the Permian it has moved mainly  
 44 vertically (Pouba & Mísař, 1961). During the Alpine orogen cycle, the SMF was reactivated as a  
 45 steeply-dipped normal fault with a horizontal component (Skácel, 2004). The neotectonic  
 46 activity of the SMF has been studied intensively over the last decades (e.g. Badura et al., 2003;  
 47 2007; Danišik et al., 2012; Ivan 1966, 1997; Krzyszkowski et al., 1995; 2000; Oberc & Dyjor,  
 48 1969; Dyjor & Oberc, 1983; Skácel, 1989; Štěpančíková et al., 2008, 2010 and citations therein).  
 49 The latest research suggests a diverse sense of slip on the SMF in different periods, but the  
 50 present-day stress field is traditionally considered to have not changed since the Pliocene.  
 51 Nevertheless, various authors assume a different sense of slip on the SMF since then. Dextral  
 52 slip is inferred e.g. in Badura et al., (2007), whereas sinistral e.g. in Nováková (2010),  
 53 Štěpančíková et al., (2008), Štěpančíková & Stemberk Jr. (2016), and possibly both senses of  
 54 slip are inferred in Stemberk Jr., et al. (2019).



55

56 **Figure 1.** The topographic relief map of the Central Sudetic Mts. using SRTM (resolution 30m;  
 57 Farr (Eds.), 2007) with the main fault zones and the main geological units. The Sudetic Marginal  
 58 fault (SMF) forms a border between the Sudetic Mts. on the SW side and the Sudetic Foreland  
 59 on the NE side. The main fault zones: BF – Biala fault zone; HPF – Hronov-Poříčí fault zone;  
 60 ISF – Intra-Sudetic fault zone; KrF – Krowiarki fault zone; SMF – Sudetic Marginal fault zone.  
 61 The main geological units: KZGM – Kłodzko-Złoty Stok granitoid massif; PG – Paczków

62 graben; SMSB – Staré Město shear belt. SnM – Śnieżnik massif; UMG – Upper Morava graben;  
63 UNKG – Upper Nysa Kłodzka graben.

64 The second important fault within the study area is the intra-mountain Bělský fault (BF),  
65 also known in Poland as the Biała, Białawka or Trzebieszowice-Biała fault. Within the study  
66 area, the Biała Łądecka River follows the fault trend. It is a fault zone comprised of several  
67 subparallel and stepping fault segments striking NW-SE. Only a few authors have dealt with this  
68 fault system (e.g. Kasza, 1964; Ivan, 1966, Buday et al., 1997, Pospíšil et al., 2019). The BF  
69 zone continues to the SE through the Hrubý Jeseník Mts. and the Nízký Jeseník Highland as a  
70 step-over fault of the Sudetic Marginal fault and forms an 8 km-wide fault zone with CO<sub>2</sub>  
71 mineral springs in Karlova Studánka, and Dolní Moravice etc. (Hynie, 1963) and Neogene and  
72 Quaternary volcanos - Uhlířský vrch hill and Venušina sopka volcano. Historical (Guterch &  
73 Lewandowska-Marciniak, 2002; Pagaczewski, 1972) and present seismicity has also been  
74 documented in this area (e.g. Špaček et al., 2006; Zedník et al., 2001). To the NW of the study  
75 area, continuation of the BF is uncertain, but it probably continues across the Upper Nysa  
76 Kłodzka Graben (UNKG) and merges with the Intra-Sudetic fault zone (ISF) or the Krowiarki  
77 fault zone (KrF) and the Hronov-Poříčí fault zone (HPF; Fig. 1).

78 Due to the fact that the sense of slip on the faults is subjected to the orientation and  
79 parameters of the regional stress field (Fossen, 2010), the stress regime in the broader area has  
80 also been intensively studied by several authors during the last few decades. Data on tectonic  
81 processes were derived from knowledge of the geological and tectonic evolution (e.g. Ziegler,  
82 1992; Dèzes et al., 2004; Ziegler & Dèzes, 2007), tectonostratigraphy (e.g. Meulenkamp et al.,  
83 2000a; 2000b; Sissingh, 2001; 2003; 2006; Rasser & Harzhauser et al., 2008), paleostress (e.g.  
84 Bergerat, 1987), volcanism (e.g. Merle & Michon, 2001), geomorphology (e.g. Badura et al.,  
85 2003), paleoseismology (e.g. Štěpančíková et al., 2010), seismology (e.g. Müller et al., 1992;  
86 Jarosiński, 2006) or extensometric measurements (e.g. Stemberk Jr. et al., 2019). Several stress  
87 field orientations were determined, but the age and time sequence of the suggested tectonic  
88 phases were not considered in detail. Nováková (2010) discovered four tectonic phases in  
89 limestone quarries near the town of Lipová Lázně. Jelínek (2008) suggested the Alpine  
90 rejuvenation of faults striking N-S to NNE-SSW and mainly W-E striking faults. Pešková et al.  
91 (2010) suggested two different tectonic phases: NE-SW compression and a transpressional  
92 tectonic regime for the Fore-Sudetic block, and NNW-SSE compression and a transtension  
93 tectonic regime since the Early Neogene for the Sudetic Mts. block. According to this work, the  
94 stress field has been more-or-less stable since the Miocene. Havíř (2002) reported WNW-ESE  
95 compression during the Neogene. The current stress field was determined by GPS measurements  
96 (e.g. Schenk et al., 2002; Kontny, 2004) as compression perpendicular to the strike of the SMF  
97 (~NE-SW compression). The current stress field was also computed by Havíř (2004), Vavryčuk  
98 et al. (2013) and Špaček et al. (2015) from focal mechanisms of micro earthquakes in broader  
99 areas as NW-SE compression. The switching of two stress/strain states based on extensometric  
100 measurements was reported by Stemberk Jr. et al. (2019) as WNW-ESE to NW-SE compression  
101 corresponding to the stress field of Western European and NNE-SSW compression  
102 corresponding to the stress field of the NW part of the Carpathian stress domain.

103 The paper deals with the Plio-Quaternary evolution of the Sudetic Mts., mainly within the  
104 study area in the RH. To determine the fault behavior in more detail, the paleostress field  
105 parameters were investigated on dated volcanic rocks. Based on the parameters of the determined

106 stress fields, theoretical fault planes with maximum shear stress and also theoretical fault planes  
107 with a tendency to dilate were determined and compared with known faults within the study area.  
108 These results and the determined orientations of the stress fields were compared to the stress  
109 fields discovered by several authors in the broader area of the European Alpine foreland and the  
110 Polish Lowlands basin since the Middle Miocene.

## 111 **1.2 Geological setting**

### 112 **1.2.1 Structure geology and tectonics**

113 The study area includes the Rychlebské hory Mts./Złote Góry Mts., which are situated in  
114 the Central Sudetes. The Sudetes represent the northeastern-most exposed fragment of the  
115 crystalline basement of the Variscan Belt in Europe, which is created by a variety of  
116 metamorphic complexes with Neoproterozoic, and Lower Paleozoic to Devonian protoliths (cf.  
117 Mazur et al., 2006; Kroner et al., 2008). They developed in the Devonian and Early  
118 Carboniferous as a result of closure of ocean basins and the amalgamation of Armorican  
119 terranes, followed by their accretion to the East European Platform (cf. Franke & Żelaźniewicz,  
120 2000; Aleksandrowski & Mazur, 2002; Kroner et al., 2008). The Central Sudetes are  
121 geologically complex and consist of several units. The study area comprises the Śnieżnik massif  
122 unit (SnM) and borders the Kłodzko-Złoty Stok granitoid massif (KZGM) to the NW and the  
123 Staré Město shear belt (SMSB) to the SE (Fig. 1, Kroner et al., 2008). The Śnieżnik massif unit  
124 consists of augen orthogneiss, migmatites, gneiss, granulites and a stratigraphically higher  
125 Stronie unit with mica-schists and belts of crystalline limestone, amphibolite and quartzite,  
126 which originated from later Variscan tectonism (Aleksandrowski et al., 2000).  
127 Thermochronological data show the post-Variscan exhumation and unroofing in the studied part  
128 of the Central Sudetes to be ~7 km (Danišík et al., 2012). During the Late Cretaceous, the  
129 broader area was buried by the thick sedimentary cover (up to ~4–7 km) of the Cretaceous Sea  
130 and rapidly exhumed to near-surface temperatures during the Late Cretaceous-Paleocene. During  
131 the Paleocene and Eocene, the Sudetic and Fore-Sudetic blocks were elevated and eroded. The  
132 planated surfaces were partially covered due to Oligocene and Miocene marine transgressions  
133 coming from the Central European Basin (Oberc, 1972). The evolution of synsedimentary  
134 Paczków-Kędzierzyn (PG, Fig. 1; PKG, Fig. 5) and Roztoki-Mokrzyszowa grabens (RMG, Fig.  
135 5) related to the SMF zone began to develop in the Latest Oligocene-Early Miocene (Dyjur &  
136 Oberc, 1983). The uplift of the Sudetic block with the formation of the Sudetic Mts. versus the  
137 Fore-Sudetic block began in the Pliocene, while the total uplift of the Sudetes since the Miocene  
138 has been estimated to be approximately 1200-1500 m. As a result, coarse syntectonic sediments  
139 of Gozdnic beds were deposited along the mountain front (Oberc, 1972; Dyjur & Oberc, 1983).  
140 The ensuing geological evolution of the study area is described in Chapter 5.

### 141 **1.2.2 Volcanism**

142 The Cenozoic volcanic activity in the broader area began in the Middle Oligocene and is  
143 divided into three volcanic phases (Birkenmajer et al., 1977). These phases indicate switching of  
144 compression phases and extension phases. The first phase occurred in the Middle Oligocene, the  
145 second phase occurred at the turn of the Oligocene and Miocene, and the third phase occurred  
146 from the Middle Miocene to the Pliocene. The volcano and its lava flows that originated during  
147 the third phase are situated in the vicinity of the village of Lutynia and Łądek Zdrój and were

148 dated by K-Ar and paleomagnetic methods as being 5.73-3.83 Ma (Birkenmajer et al., 2002;  
149 Cajz et al., 2012; Ulrych et al., 2013). Due to their Pliocene age, we have chosen them as being  
150 suitable for studying the Pliocene and younger paleostresses. The kinematic indicators were  
151 studied on four sites (Fig. 2, see Fig. 1 or Fig. 7 for their locations).

152 The **Čedičový vrch hill** site (CH, Fig. 2 - 2; N 50.35500°, E 016.92282°) is characterized  
153 as lava flows exposed in an old quarry on the main ridge of the Rychlebské hory Mts. (RH)  
154 approximately 3 km to the NE of Łądek Zdrój. A sequence of two lava flows is separated by a 2  
155 m-thick layer of pyroclastic material. The volcanic rock has been classified as nephelitic basanite  
156 with olivines and xenoliths, which form volcanic columns (Fediuk & Fediuková, 1989).  
157 According to Ulrych et al., 2013, the age of lava flows is 5.73 Ma ± 0.23 Ma. To-date,  
158 measurement of a striae data set has only been performed in the uppermost 5-7 m thick lava  
159 flow.

160 The **Czerne Urwisko/Ślupy Bazaltowe** site (CU, Fig. 2 - 4; N 50.36378°, E 016.90152°) is  
161 situated approximately 1.5 km to the NE of Łądek Zdrój near Lutynia. The rock has been  
162 classified as grey basanite rock, which creates a 15-20 m-thick lava flow, with subvertical  
163 volcanic columns that are 0.5–1 m in diameter. The rocks are exposed in an old pit and are from  
164 the Early Pliocene-Zanclean (3.83 Ma ± 0.17 Ma) according to K-Ar dating carried out by  
165 Birkenmajer et al. (2002).

166 The **Lutynia quarry** site (LQ, Fig. 2 - 1; N 50.35957°, E 016.91118°) is situated 2.5 km to the  
167 NE of Łądek Zdrój near Lutynia. It is presented as a volcanic plug dated to the Early Pliocene-  
168 Zanclean (4.56 Ma ± 0.20 Ma) after Birkenmajer et al., (2002). The site is an active quarry with  
169 walls 15-30 m high and volcanic columns 0.5 – 2 m in diameter.

170 The **Szary Kamień** site (SZ, Fig. 2 - 3a; N 50.35202°, E 016.8642°) is located approximately 1  
171 km to the WNW of Łądek Zdrój. The lava flow is characterized as irregular volcanic columns,  
172 0.5-1m in diameter and is exposed in an old pit. According to Berger (1932) and Walczak  
173 (1954), the basanite flow overlays fluvial gravels of the Biała Łądecka river terrace from the  
174 Pliocene or Early Pleistocene. Later research by Birkenmajer et al., (2002) using K-Ar



175 determined the age of the volcanic rocks as being from the Late Miocene – Messinian (5.46 Ma  
 176  $\pm 0.23$  Ma).



177  
 178 **Figure 2.** The photomosaic of the volcanic rocks sites in Lutynia / Łądek Zdrój area. 1 – the  
 179 volcanic plug in the Lutynia quarry (LQ); 2 – the fragment of the lava flow on the Čedičový vrch  
 180 hill site (CH); 3a – the fragment of the lava flow on the Szary Kamień site (SK); 3b – example of  
 181 the slickenside with two sets of striae on the Szary Kamień site; 4 – the fragment of the lava flow  
 182 on the Czarne Urwisko site (CU).

## 183 2 Methods

184 The volcanic rocks are intensively fractured in the all of the studied sites. Movement  
 185 along the fault planes is demonstrated by the presence of kinematic indicators (e.g. slickensides,  
 186 striae, calcite steps, stylolites, etc.). In this work, we collected kinematic information from  
 187 slickensides with striae (Fig. 2 - 3b). The datasets of striae on volcanic outcrops near Łądek  
 188 Zdrój and Lutynia with known radiometric K/Ar ages after Birkenmajer et al. (2002), Cajz et al.  
 189 (2012) and Ulrych et al. (2013) were used as input data for the application of paleostress  
 190 computational methods to determine the regional stress field characteristics during the Pliocene  
 191 and Quaternary.

### 192 2.1 Parameters of the kinematic indicators

193 Each dataset from each site includes several measured kinematic characteristics of striae  
 194 on slickensides. They are described by two quantities: orientation of the fault plane with  
 195 components  $A_p$  (fault strike/trend),  $\Phi_p$  (fault dip/plunge), and orientation of the striae with  
 196 component  $A_s$  (striae strike/trend),  $\Phi_s$  (striae dip/plunge). Several measurements were  
 197 supplemented by the sense of slip on the plane (normal/reverse or sinistral/dextral). In some

198 cases, the slickensides contain multiple generations of striae. The superposition of these multiple  
199 generations of striae was also recorded (Sperner & Zweigel, 2010).

## 200 **2.2 Analysis of the stress parameters**

201 The paleostress analysis is based on continuum mechanics, which estimates the  
202 parameters of a slip on arbitrary slickensides for the known parameters of stress orientation  
203 (Angelier et al., 1982; Angelier, 1989). In practice, the inverse situation is solved where the  
204 principal parameters of the stress that caused the later measured slips on the slickensides  
205 recorded as striae are calculated from the measured slip orientation on several slickensides. The  
206 principal stress parameters are expressed as a total stress tensor. In this work, a reduced stress  
207 tensor was calculated, which approximates the total stress tensor neglecting the isotropic part of  
208 the crustal stress (Angelier, 1989, 1994). The approximation can be used because the site is  
209 located in very shallow parts of the Earth's crust.

210 Processing of the datasets consisted of two phases. During the first phase, all of the  
211 datasets from the individual sites were processed in the updated software ROCK2014 (Málek et  
212 al., 1991). This software automatically separates datasets of measured striae to statistic groups  
213 with similar parameters. It uses the polyphase analysis numerical method after Angelier (1994)  
214 to determine the stress field orientation from the kinematic characteristics of the individual striae.  
215 The misfit angle  $\alpha$  (Tab. 1) between the observed striae on the slickenside and theoretical ones,  
216 which correspond to a computed stress state, was also calculated (Hippolyte et al., 2012). In this  
217 work, a misfit angle of less than  $25^\circ$  is assumed as a good agreement. A heterogeneous data set  
218 of striae is divided into homogenous subsets – paleostress states (e.g. SK-1, LQ-2, etc., Tab. 1,  
219 Fig. 3) based on a comparison of misfit angles with all of the individual stress states. The data  
220 distribution of misfit angles grouped into  $5^\circ$  intervals is presented on histograms in Fig. 3 and  
221 represents the quality indicator of the determined paleostress states. The reliability and precision  
222 of the method used are discussed in e.g. Coubal et al. (2015).

223 During the second phase, paleostress states were compared using an approximative  
224 method of P and T-axes in the FaultKin 7 software (cf. Marrett & Allmendinger, 1990;  
225 Allmendinger et al., 2012). Paleostress patterns (marked as PPA-PPF) were defined and  
226 visualized as stereo-plots (Fig. 4) and the stress field parameters presented in Tab. 2a and Tab  
227 2b. The time aspect was also considered during the comparison.

228 The reduced stress tensor, which characterizes the single paleostress state/pattern, has the  
229 following principal parameters: direction of its principal stresses ( $\sigma_1$  – maximum,  $\sigma_2$  –  
230 intermediate and  $\sigma_3$  – minimum) and ratio  $\Phi = (\sigma_2 - \sigma_3) / (\sigma_1 - \sigma_3)$  describing the difference  
231 between the magnitudes of the principal stresses (Angelier, 1994). The values of  $\Phi$  range from 0  
232 (uniaxial compression) to 1 (uniaxial extension). The  $\Phi$  ratio parameter varies depending on the  
233 amount of data (n) in the individual paleostress state/pattern (Málek et al., 1991). Paleostress  
234 states/patterns with sub-horizontal  $\sigma_1$  were marked as compressional, and episodes with  
235 subhorizontal  $\sigma_3$  were marked as extensional (cf. Stemberk Jr. et al., 2019).

236 The determined stress field parameters were then used to determine the parameters of  
237 fault planes, where the normal component is the lowest and the shear stress component is the  
238 highest. According to the Coulomb stress criterion, these planes may have been activated by slips



239 during single paleostress patterns (Moriss et al., 1996; Fossen, 2010). There are two planes, with  
240 theoretical orientation  $\pm 45^\circ$  from  $\sigma_1$  and transect in  $\sigma_2$ . In practice, based on empiric  
241 observations, the angle between  $\sigma_1$  and both the planes is lower. In this work, we used as a good  
242 approximation of the value of angle  $\pm 30^\circ$  (Ramsay & Huber, 1987; Fossen, 2010). Similarly, the  
243 planes that are perpendicular to the  $\sigma_3$  axis tend to dilate (Ramsay & Lisle, 2000) (Fig. 7). The  
244 computed theoretical fault planes (Fig. 4) were compared with published faults (fault segments  
245 with uniform strikes) within the study area in each paleostress pattern. The faults were collected  
246 from map sources: Don et al. (2003), Müller and Čurda (2003), Skácel (1989), Skácelová  
247 (1992a; 1992b; 1997), map portal of the Czech Geological Survey, geological maps of the  
248 Sudetes: 902C-Trzebieszowice (Cwojdzinski, 1977), 902D-Lądek Zdrój (Gierwielanic, 1968),  
249 934A-Stronie Śląskie (Cwojdzinski, 1981) and 934B-Strachocin, Bielice (Cymerman &  
250 Cwojdzinski 1984). Unfortunately, there is no detailed information about fault geometries, only  
251 about the strike. According to Skácel (1963) and Ivan (1966), most of the faults in the broader  
252 area are nearly sub-vertical, but the fault dip orientation and angle are unknown. We only  
253 approximated the issue of the reactivation of the faults to the distribution of the fault strikes,  
254 where the dip angle and dip direction were not considered. When the orientation of the fault  
255 differs less than  $\pm 10^\circ$  from theoretical one, the fault was marked as a fault with a tendency to  
256 slip/dilate. A fault with a strike difference of  $\pm 5^\circ$  from the theoretical one was marked as a fault  
257 with a high tendency to slip/dilate (Fig. 7).

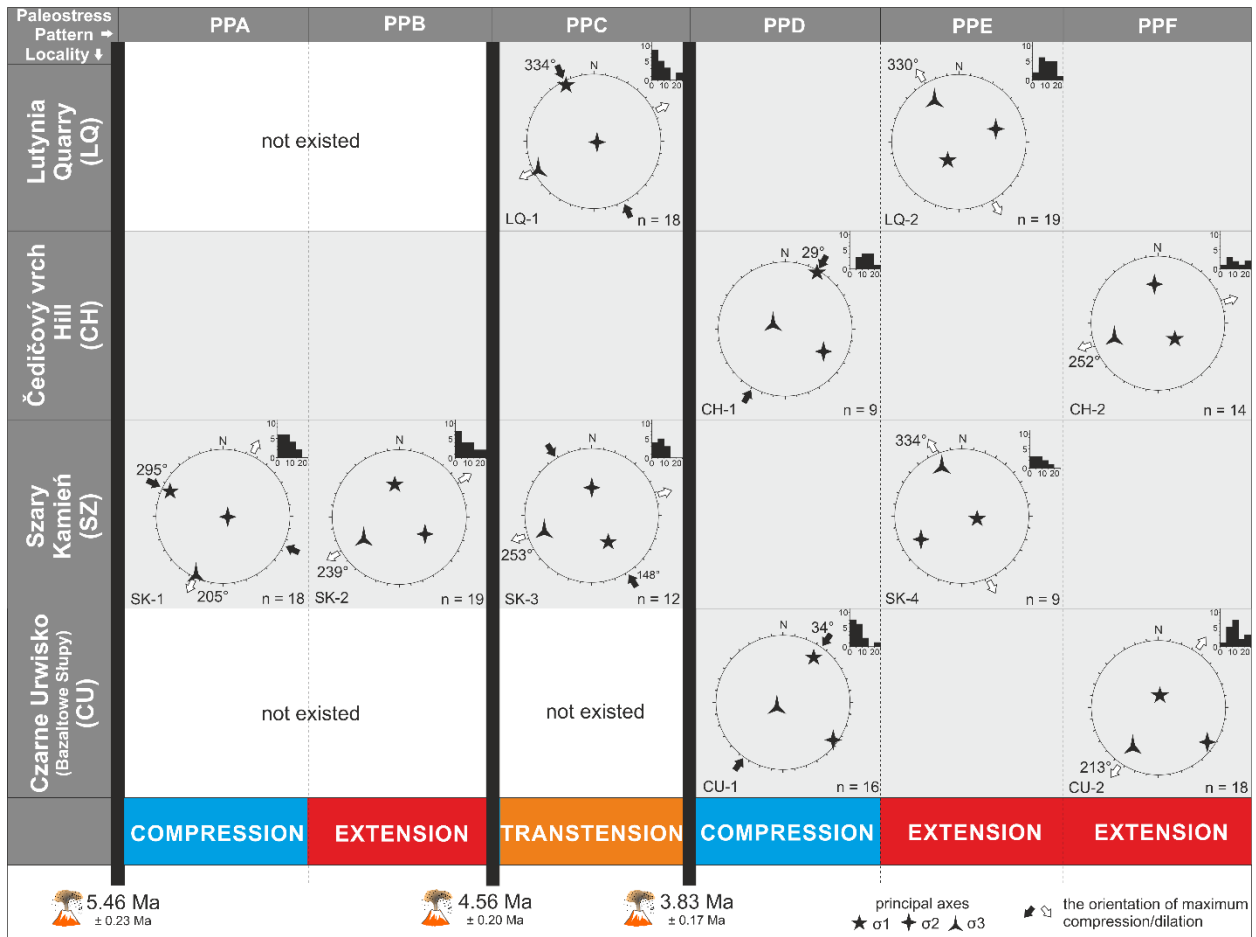
258 Moreover, based on the mechanics (e.g. Angelier, 1994), the stress field causes the same  
259 sense of slip on all of the parallel faults at all of the different scales. The block diagrams in Fig. 4  
260 show the determined slips on slickensides in volcanic rocks applied to a larger scale of relief  
261 evolution in the individual paleostress patterns.

262 The important aspect used in this work is the time-sequence of the determined paleostress  
263 patterns. The first method used is relative timing. This is based on the fact that the registered data  
264 contain a sequence of variously superimposed generations of striae on reactivated slickensides.  
265 The second method, sub-geochronological timing, is based on studying the kinematics of brittle  
266 structures and their relationships with geochronologically dated rocks. In this case, the Tertiary  
267 basaltoid volcanic rocks dated by the K-Ar dating method carried out by Birkenmajer et al.  
268 (2002), Cajz et al. (2012) and Ulrych et al. (2013) were used. It is possible to suggest the time  
269 period of the paleostress pattern action based on whether it is disrupting volcanic rocks of  
270 different ages or not. The dating of volcanic rocks comes with certain inaccuracies, but in  
271 comparison with commonly used geological timing based on disrupting sediment formations, it  
272 is a significant refinement of the time periods.

### 273 **3 Results**

274 Based on the similarity of the stress tensor parameters and their time-superposition, six  
275 groups of paleostress patterns were identified and marked as PPA-PPF (Fig. 3; Fig. 4). The  
276 paleostress patterns are sorted chronologically. All of the presented paleostress patterns are from

277 the Late Miocene to Pleistocene. The age is estimated as an interval between the dated volcanic  
 278 events (after Birkenmajer et al., (2002), Ulrych et al. (2013) and Cajz et al. (2012)).

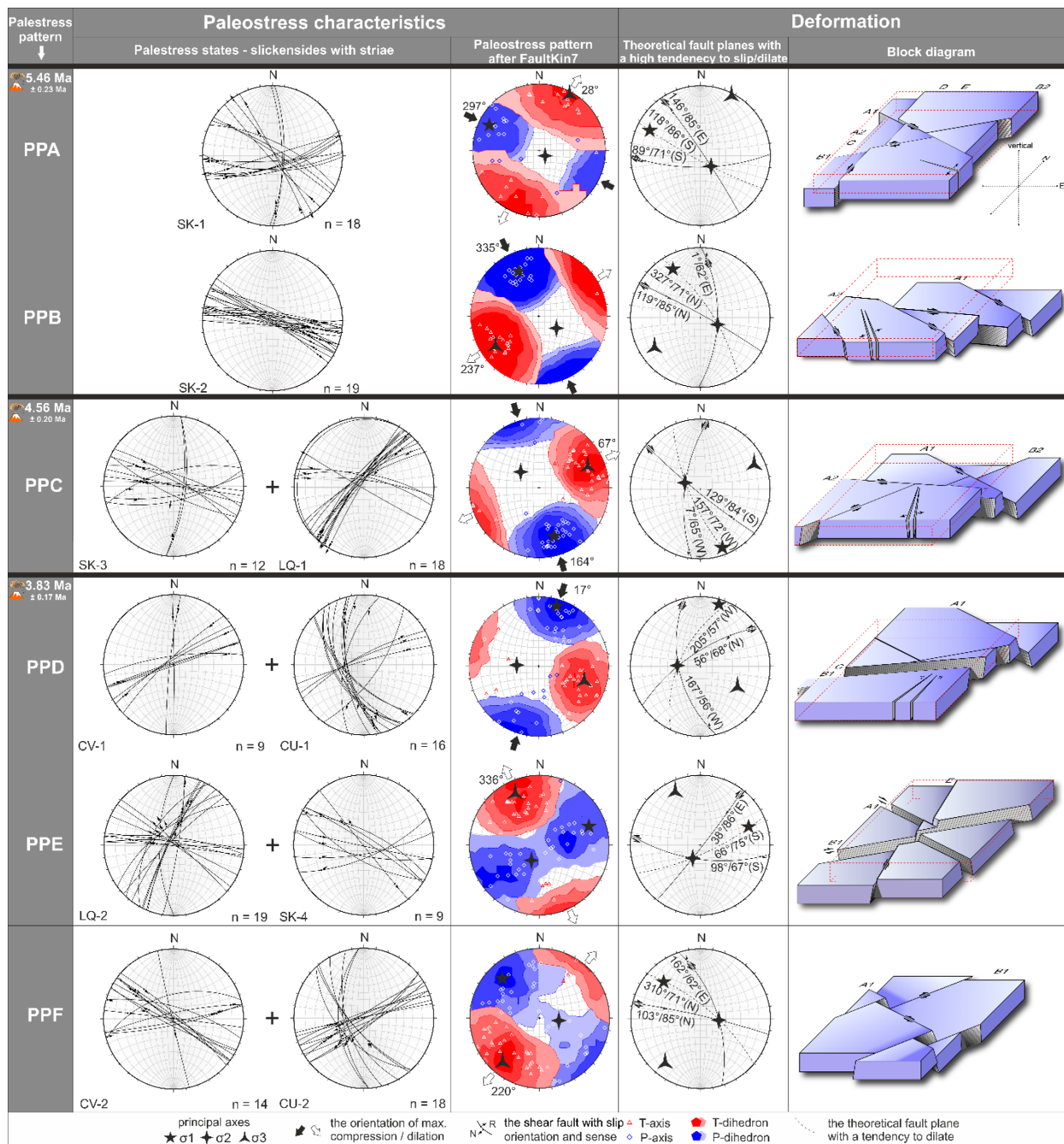


279

280 **Figure 3.** The paleostress states (e.g. CU-2) after the updated software ROCK2014 (Málek et al.,  
 281 1991) and the paleostress patterns (e.g. PPA) sorted by sites in time sequence. The histograms in  
 282 individual paleostress states show the data quality based on the misfit angle in range 0°-25°; n =  
 283 sum of striae in the individual paleostress states.

Paleostress state	σ1		σ2		σ3		Φ	n	Q
	Tr.	Pl.	Tr.	Pl.	Tr.	Pl.			
CU-1	34°	32°	335°	29°	266°	40°	0.278	16	A
CU-2	15°	58°	121°	20°	213°	21°	0.698	18	A
CH-1	29°	1°	120°	23°	295°	67°	0.145	9	C
CH-2	132°	52°	355°	30°	252°	21°	0.848	14	B
LQ-1	334°	4°	103°	84°	243°	4°	0.775	18	A
LQ-2	213°	55°	71°	30°	330°	18°	0.638	19	A
SK-1	295°	8°	94°	82°	205°	3°	0.294	18	A
SK-2	148°	40°	0°	45°	253°	17°	0.288	19	A
SK-3	352°	38°	123°	41°	239°	27°	0.816	12	B
SK-4	100°	62°	241°	20°	334°	11°	0.756	9	C

284 **Table 1.** The parameters of the paleostress states. Tr. – trend; Pl. – plunge;  $\Phi$  – the ratio of the  
 285 stress differences  $\Phi = (\sigma_2 - \sigma_3)/(\sigma_1 - \sigma_3)$ ; n – number of events forming homogenous subset; Q –  
 286 quality estimator for the fault-slip data datasets. The grade of the quality estimator is based on  
 287 the number of events forming the homogenous dataset: A – 15 or more events (excellent), B –  
 288 10-14 events (good), C – 4-9 events (fair), D – 4 events (poor) (after Coubal et al. 2015).



289 **Figure 4.** The results of the fault slip dynamics analysis. Overall character of the observed  
 290 paleostress patterns. First column shows the stereo-plots of the slickensides with striae in the  
 291 individual paleostress states (e.g. SK-1), which belong to the same paleostress pattern (e.g. PPA);  
 292

293 n = sum of striae on slickensides in the individual paleostress states. Second column shows  
 294 beach ball charts of the P-axis and the T-axis orientation after the software FaultKin 7  
 295 (Allmendinger et al., 2012). Third column shows the stereographic plots with the planes with  
 296 maximum shear stress/a high tendency to slip (after Ramsay & Huber, 1987; Fossen, 2010) and  
 297 the planes/fissures with a high tendency to open (Ramsay & Lisle, 2000). Fourth column shows  
 298 the block diagrams created based on the observed slickensides in the volcanic rocks and its  
 299 deformation caused by the paleostress field action.

Paleo-stress pattern	$\sigma_1$		$\sigma_2$		$\sigma_3$		n	Q	Included paleostress states
	Tr.	Pl.	Tr.	Pl.	Tr.	Pl.			
PPA	297°	17°	131°	72°	28°	4°	18	A	SK-1
PPB	335°	22°	111°	60°	237°	19°	19	A	SK-2
PPC	164°	19°	296°	64°	67°	18°	30	A	LQ-1, SK-3
PPD	17°	11°	271°	55°	115°	33°	25	A	CH-1, CU-1
PPE	71°	18°	208°	66°	336°	15°	28	A	LQ-2, SK-4
PPF	319°	23°	94°	60°	220°	19°	32	A	CH-2, CU-2

300 **Table 2a.** The parameters of the paleostress patterns (part 1). Str. – strike; Tr. – trend; Pl. –  
 301 plunge; N – normal; R – reverse; S – sinistral; D – dextral; n – number of events forming  
 302 homogenous subset; Q – quality estimator for fault-slip data subset. The grade of the quality  
 303 estimator is based on the number of events forming the homogenous subset: A – 15 or more  
 304 events (excellent), B – 10-14 events (good), C – 4-9 events (fair), D – 4 events (poor) (after  
 305 Coubal et al., 2015).

Paleo-stress pattern	Theoretical plane 1 with maximum shear stress		Theoretical plane 2 with maximum shear stress		Theoretical plane with a tendency to open
	Plane (Str./Dip)	Striae (Tr./Pl.)	Plane (Str./Dip)	Striae (Tr./Pl.)	Plane (Str./Dip)
PPA	146°/85° to E	327°/18° S/N	89°/71° to S	266°/13° D/N	118°/86° to S
PPB	1°/62° to E	5°/9° S/N	119°/85° to N	302°/30° D/R	327°/71° to E
PPC	129°/84° to S	132°/24° D/R	7°/65° to W	191°/7° S/N	157°/72° to W
PPD	56°/68° to N	45°/26° S/R	167°/56° to W	171°/6° D/R	205°/57° to W
PPE	38°/86° to E	40°/23° D/R	98°/67° to S	101°/7° S/N	66°/75° to S
PPF	103°/85° to N	286°/29° D/R	162°/62° to E	347°/10° S/N	310°/71° to N

306 **Table 2b.** The parameters of the paleostress patterns (part 2). Str. – strike; Tr. – trend; Pl. –  
 307 plunge; N – normal; R – reverse; S – sinistral; D – dextral.

### 308 3.1 Late Miocene-Early Pliocene WNW-ESE compression - PPA

309 This compression phase was constructed based on a dataset containing 18 striae on  
 310 slickensides, and was only identified at the Szary Kamień site as paleostress state SK-1 (Fig. 4).  
 311 The compression must have appeared between  $5.46 \text{ Ma} \pm 0.23 \text{ Ma}$  and  $4.56 \pm 0.20 \text{ Ma}$ . The  
 312 orientation of the principal axes is subhorizontal  $\sigma_1$  (297°/17° after FaultKin7; trend/plunge) and  
 313 subhorizontal  $\sigma_3$  (28°/4°). The set of planes with maximum shear stress is oriented subvertically  
 314 89°/71° (strike/dip) to the S as a dextral/normal fault and 146°/85° to the E as a sinistral/normal  
 315 fault. The plane with the highest tendency to open is oriented subvertically 118°/86° to the S.  
 316 This stress field configuration produced subsidence of the western blocks towards the eastern  
 317 ones. The NW-SE to WNW-ESE oriented faults had a sinistral sense of movement with no

318 vertical component, and the WSW-ESE oriented faults had a dextral sense of movement, also  
 319 without any vertical component. A block diagram with a schematic sketch of the block  
 320 deformations is presented in Fig. 4.

### 321 **3.2 Late Miocene-Early Pliocene NE-SW extension - PPB**

322 This extension phase was reconstructed based on a dataset containing 19 striae on  
 323 slickensides. It was only identified at the Szary Kamień site as a paleostress state SK-2 (Fig. 4).  
 324 The extension must have appeared between  $5.46 \text{ Ma} \pm 0.23 \text{ Ma}$  and  $4.56 \pm 0.20 \text{ Ma}$  (Late  
 325 Miocene-Early Pliocene), following the previous phase. The orientation of the principal axes is  
 326  $\sigma_1$   $335^\circ/22^\circ$  and  $\sigma_3$   $237^\circ/19^\circ$ . The planes with the maximum shear stress are oriented  $1^\circ/62^\circ$  to  
 327 the E as a sinistral/normal fault and  $119^\circ/85^\circ$  to the N as a dextral/reverse fault. The plane with  
 328 the highest tendency to dilate has an orientation of  $327^\circ/71^\circ$  to the E. This stress field has  
 329 produced a complicated structure with uplifted northern blocks towards the southern ones.  
 330 Moreover, the eastern blocks are subsiding against the western blocks separated by subvertical  
 331 N-S trending faults. The faults striking WNW-ESE to WSW-ESE have a dextral sense of  
 332 movement (see the block diagram in Fig. 4).

### 333 **3.3 Early Pliocene transtension - ENE-WSW extension/NNW-SSE compression - PPC**

334 This phase has no dominant extension/compression component and was constructed from  
 335 a dataset containing 30 striae on slickensides. It was identified at the Szary Kamień site as a  
 336 paleostress state SK-3 and in the Lutynia active quarry as a paleostress state LQ-1 (Fig. 4). The  
 337 phase must have appeared between  $4.56 \pm 0.20 \text{ Ma}$  and  $3.83 \pm 0.17 \text{ Ma}$  (Early Pliocene). The  
 338 orientation of the principal axes is  $\sigma_1$   $164^\circ/19^\circ$  and  $\sigma_3$   $67^\circ/18^\circ$ . The planes with the maximum  
 339 shear stress are oriented  $129^\circ/84^\circ$  to the S as a dextral/reverse fault and  $7^\circ/65^\circ$  to the W as a  
 340 sinistral/normal fault. The plane with the highest tendency to dilate has an orientation of  
 341  $157^\circ/72^\circ$  to the W. This stress field produced the subsidence of the northern blocks against the  
 342 southern ones on the E-W to NW-SE striking faults, also with a dextral sense of movement. The  
 343 sinistral faults striking NE-SW were also activated (see the block diagram in Fig. 4).

### 344 **4.4 Late Pliocene NNE-SSW compression - PPD**

345 This compression phase was constructed based on a dataset containing 27 striae on  
 346 slickensides. It was identified in the Čedičový vrch hill inactive quarry as a paleostress state CH-  
 347 1 and on the Czarne Urwisko/Bazaltowe Słupy outcrop as a paleostress state CU-1. The phase  
 348 must have appeared after  $3.83 \pm 0.17 \text{ Ma}$  (Early Pliocene) but before the PPE (see below). The  
 349 orientation of the principal axes is  $\sigma_1$   $17^\circ/11^\circ$  and  $\sigma_3$   $115^\circ/33^\circ$ . The planes with maximum shear  
 350 stress are oriented  $56^\circ/68^\circ$  to the N as a sinistral/reverse fault and  $167^\circ/56^\circ$  to the W as a  
 351 dextral/reverse fault. The plane with the highest tendency to dilate has an orientation of  $205^\circ/57^\circ$   
 352 to the W. This stress field configuration produced the horst-like relief along the faults striking  
 353 ENE-WSW and NW-SE (see the block diagram in Fig. 4).

### 354 **4.5 Late Pliocene-Early Pleistocene NW-SE extension - PPE**

355 This extension phase was constructed based on a dataset containing 28 striae on  
 356 slickensides. It was identified on the Szary Kamień outcrop as a paleostress state SK-4 and in the  
 357 Lutynia active quarry as a paleostress state LQ-2. The phase must have appeared after  $3.83 \pm$

358 0.17 Ma (Early Pliocene), after the PPD and before the PPF (see below). The orientation of the  
 359 principal axes is  $\sigma_1$  17°/11° and  $\sigma_3$  115°/33°. The planes with maximum shear stress are oriented  
 360 56°/68° to the N as a sinistral/reverse fault and 167°/56° to the W as a dextral/reverse fault. The  
 361 plane with the highest tendency to dilate has an orientation of 66°/75° to the S. This stress field  
 362 caused subsidence of the southern blocks against the northern ones along the faults striking NW-  
 363 SE and NE-SW, both with a dextral horizontal component. In addition, the western blocks are  
 364 subsiding against the eastern ones along the N-S striking faults with a sinistral horizontal sense  
 365 of movement (see the block diagram in Fig. 4).

#### 366 **4.6 Late Pliocene-Early Pleistocene NE-SW extension - PPF**

367 This extension phase was constructed based on a dataset containing 31 striae on  
 368 slickensides. It was identified in the Čedičový vrch hill inactive quarry as a paleostress state CH-  
 369 2 and on the Czarne Urwisko/Bazaltowe Słupy outcrop as a paleostress state CU-2. This phase  
 370 must have appeared after  $3.83 \pm 0.17$  Ma (Early Pliocene) and after the PPE phase. The  
 371 orientation of the principal axes is  $\sigma_1$  319°/23° and  $\sigma_3$  220°/19°. The planes with maximum  
 372 shear stress are oriented 103°/85° to the N as a dextral/reverse fault and 162°/62° to the E as a  
 373 sinistral/normal fault. The plane with the highest tendency to dilate has an orientation of  
 374 310°/71° to the N. This stress field configuration caused subsidence of the northeastern blocks  
 375 against the southwestern ones along the faults striking NW-SE with a sinistral horizontal  
 376 component (see the block diagram in Fig. 4).

377 It can be assumed that the stress parameters and orientations of the activated faults have  
 378 changed several times since the Late Miocene to Early Pleistocene.

## 379 **4 Discussion**

380 The paleostress events of the Late Miocene to Quaternary observed in the area of  
 381 Lutynia/Lądek Zdrój were compared with the stress field of broader regional or sub-continental  
 382 dimensions.

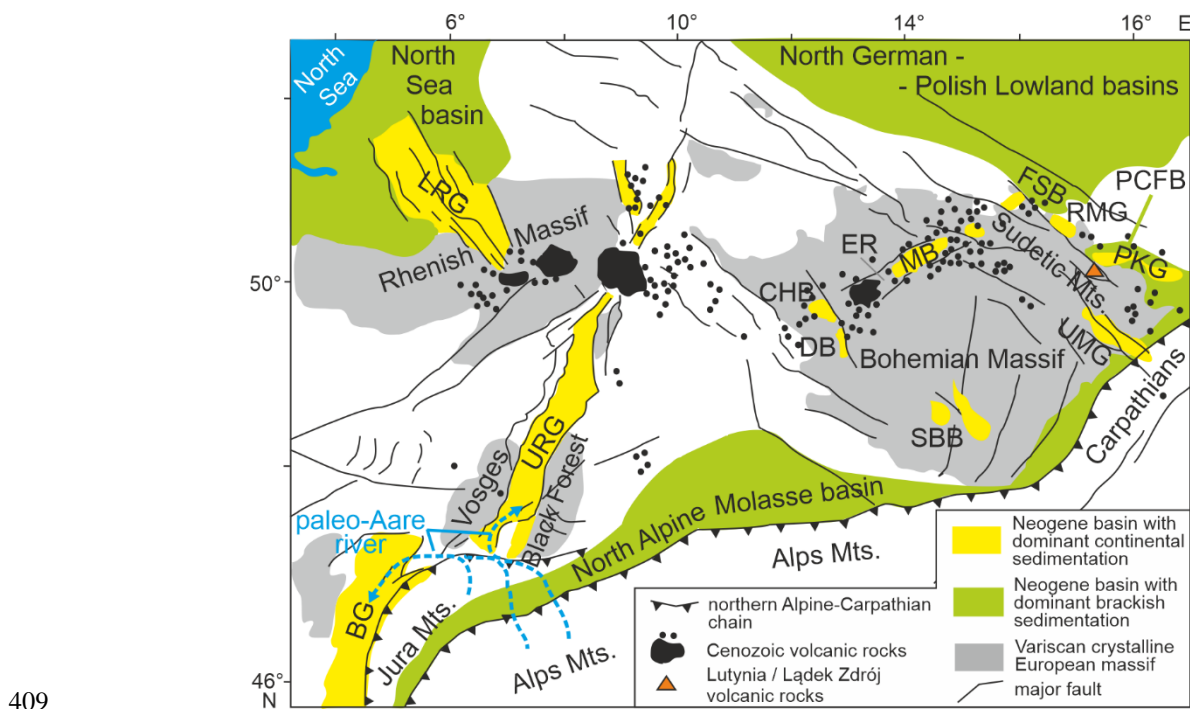
### 383 **4.1 The character of tectonic evolution of the Alpine and North Carpathian forelands since** 384 **the Middle Miocene to date**

385 The present N to NW oriented compressional stress regime of the Alpine and North  
 386 Carpathian forelands reflects a combination of forces related to the continued counterclockwise  
 387 convergence of the Africa-Arabia plates with Europe, and consequently collisional interaction of  
 388 the Alpine orogen with its foreland, and the North Atlantic ridge push. The interplay of stress  
 389 impulses generated by both the above- mentioned sources has created the paleostress/tectonic  
 390 history of the European Alpine foreland (EAF) at least during the Pliocene and Quaternary  
 391 (Müller et al., 1992; Dèzes et al., 2004; Ziegler & Dèzes, 2007). The switching of compressional  
 392 and extensional pulses derived from both sources has caused the movement of large crustal  
 393 blocks or whole regions in the Alpine foreland. The periods of uplift followed by erosion  
 394 switched with periods of dominant subsidence followed by sediment deposition. In addition, the



395 periods of increased frequency of volcanic events indicate the lower intensity of compression (cf.  
 396 Fossen, 2010).

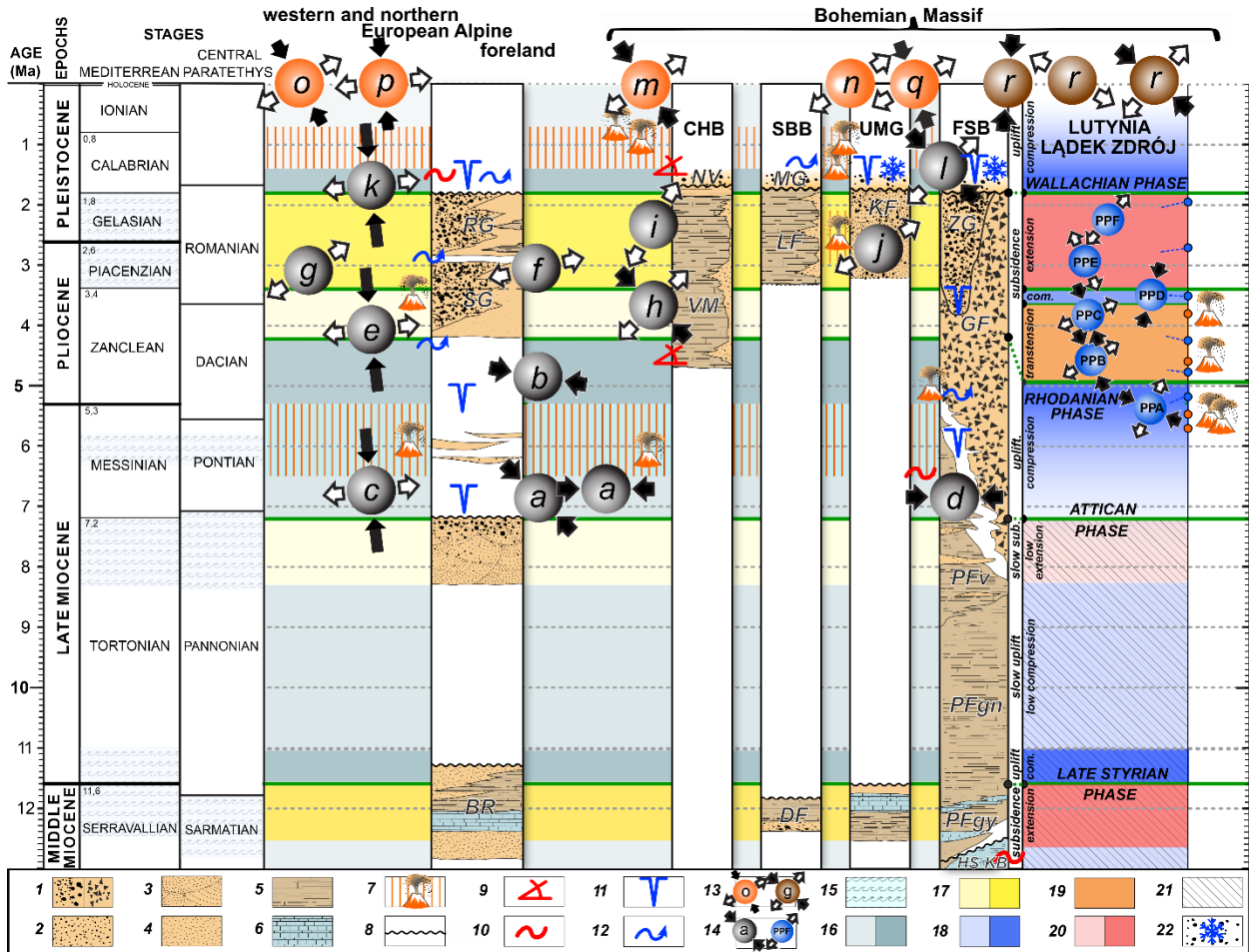
397 The European Alpine foreland can be divided into three zones. The first zone represents  
 398 the narrow stripe-shape zone in front of the Alps, which matches more-or-less with the North  
 399 Alpine Molasse basin (Fig. 5). This zone coincides with the rapid elevation of the Alps since the  
 400 Middle Miocene (Rasser & Harzhauser, 2008). The second zone comprises the southern part of  
 401 the western- and middle-EAF, which coincides with the zone of Variscan crystalline European  
 402 massifs (Fig. 5). This zone is characterized as sub-continually uplifting crystalline massifs,  
 403 which are separated by simultaneous episodic subsidence of the European Cenozoic Rift  
 404 System (ECRIS; Dèzes et al, 2004; Ziegler & Dèzes, 2007, Fig. 5). The Bohemian Massif,  
 405 including the study area, is situated within this zone. The third zone is represented by the  
 406 northern/outer part of the EAF marked by the North Sea-North German basin and Polish  
 407 Lowlands basins (Fig. 5). The continuous subsidence in this zone has been active since the  
 408 Miocene (Ziegler & Dèzes, 2007).



410 **Figure 5.** The schematic map of the main Cenozoic tectonic features in the European Alpine  
 411 foreland (modified after Dèzes et al., 2004; Dyjor, 1981; Sissingh, 2006). FSB – Fore-Sudetic  
 412 block; PCFB – Polish Carpathian Foredeep basin; the Neogene basins: BG – Bresse graben,  
 413 CHB – Cheb basin, DB – Domažlice basin, ER – Eger rift, LRG – Lower Rhine graben, MB –

414 Most basin, PKG – Paczków – Kędzierzyn graben, RMG – Roztoki – Mokrzeszowa graben,  
 415 SBB – South Bohemian basins, UMG – Upper Morava graben, URG – Upper Rhine graben.

416 Fig. 6 includes a comparison of the main tectonic events within the western and northern  
 417 European Alpine foreland (WNEAF) with paleostress patterns in the Bohemian massif and the  
 418 ones derived in the Lutynia/Lądek Zdrój area since the Middle Miocene to Pleistocene.



419

420 **Figure 6.** The comparison of the tectonostratigraphic evolution, the volcanic activity and the  
 421 paleostress events within the Western and Northern European Alpine foreland (WNEAF) and the  
 422 Bohemian Massif observed by other authors (the comprehensive symbols of the stress marked as  
 423 a, b, ...) with the paleostress events observed within the Lutynia / Lądek Zdrój area (the  
 424 comprehensive symbols of the stress marked as PPA-PPF) since Middle Miocene to-date. The  
 425 compared areas: WNEAF – with emphasis on the evolution in the Upper Rhine Graben and the  
 426 Jura Mts.; the Bohemian Massif – with emphasis on the evolution in the CHB – Cheb Basin,  
 427 SBB – South Bohemian basins, UMG – Upper Moravia graben and FSB – Fore-Sudetic block. 1  
 428 – gravels, sedimentary breccia; 2 – alluvial mostly clastic sediments; 3 – fluvial sands; 4 –  
 429 lacustrine mostly sandy deposits; 5 – terrestrial shales; 6 – marine and brackish sediments  
 430 (mostly shales); 7 – volcanic event; 8 – erosional boundary (hiatus); 9 – angular unconformity;  
 431 10 – folding; 11 – deep erosion; 12 – river reconfiguration; 13 – comprehensive symbols of the  
 432 present-day stress, for explanation and reference see chapter 5 based on letters; 14 –

433 comprehensive symbols of the paleostress, for the explanation and the references see chapter 4  
 434 based on letters; 15 – period with dominant sedimentation and frequent marine ingressions  
 435 within the WNEAF; The tectonic regimes deduced from the tectonostratigraphic evolution and  
 436 the paleostress analysis: 16 – slow / fast uplift; 17 – slow / fast subsidence; The stress states  
 437 deduced: 18 – low / intensive compression, 19 – transtension (strike-slip regime); 20 – extension,  
 438 low or intensive.; 21 – Tectonic regimes deduced from tectonostratigraphic evolution only; 22 –  
 439 glacial or glacialfluvial deposits. The sedimentary formations (for the explanation and the  
 440 references see chapter 4): BR – Bois de Raube formation, DF – Domanín formation, GF –  
 441 Gozdnica formation, HS – Henryk seam; KB – Kędzierzyn and Krakowiec beds; KF – Křelov  
 442 formation, LF – Ledenice formation, MG – Moldavite Gravels, NV – Nová Ves formation, PFgr  
 443 – Poznań formation – green clay, PFgy – Poznań formation – grey clay, PFv – Poznań formation  
 444 – variegated clay, RG – Rhine or Alpine gravels, SG – Sungau gravels, VM – Vonšov member  
 445 as a part of Vildštejn formation, ZG – Ziebice group.

#### 446 **4.1.1 Middle-Late Miocene subsidence/extension (until 11 Ma)**

447 During the Middle Miocene, the WNEAF, including the Bohemian Massif, was located at  
 448 a low elevation and the extensional regime with subsidence and sediment accumulation was  
 449 dominant here. Evidence of the subsidence was documented by lacustrine sediments (Domanín  
 450 formation; DF, Fig. 6) in the Southern Bohemian basins (SBB, Fig. 5; Malkovský, 1979; Pešek,  
 451 ed., 2010). The fluvio-lacustrine sediments with a marine ingression record of the Lower  
 452 Badenian (15 – 16.4 Ma) are also preserved in the Upper Morava graben (UMG, Fig.5; Pešek,  
 453 ed., 2010; Růžička, 2016; Špaček et al., 2015). The last marine ingression in the North Alpine  
 454 Molasse basin occurred during the Late Serravallian and sedimented here as the Bois de Raube  
 455 formation (ca. 11 Ma; Rasser & Harzhauser et al., 2008; BR, Fig. 6). In the Cheb basin (CHB,  
 456 Fig. 5) in the northwestern Bohemian Massif, the youngest Miocene sediments (Cypris  
 457 formation) are preserved from the period 21.3-17 Ma (Bucha et al., 1990). While the Miocene  
 458 sedimentation in the basins of the Bohemian Massif terminated around 17 Ma, it ended in the  
 459 peripheral basins around the Bohemian Massif around 13-14.8 Ma (Malkovský, 1979; Pešek, ed.,  
 460 2010).

461 The area of the Sudetic Mts., where the Rychlebské hory Mts. are situated, underwent the  
 462 uplift during that period, in contrast to the Fore-Sudetic block (FSB, Fig.5), where the  
 463 continental clastic sediments were deposited under brackish or shallow marine conditions. The  
 464 area of the Fore-Sudetic block, mainly in Paczków-Kędzierzyn and Rostoki-Mokrzyszowa  
 465 grabens (Ondra, 1968), subsided mainly during the Serravallian (Rasser & Harzhauser et al.,  
 466 2008). The Paczków-Kędzierzyn grabens (PKG, Fig. 5) were covered by the Paratethys Sea  
 467 coming from the Polish Carpathian Foredeep basin (PCFB, Fig. 5), where 300 m-thick layers of  
 468 clayey, silty and sandy fluvial and deltaic material with coal and lignite seams were deposited  
 469 (Gabriel et al., 1982) as Kędzierzyn and Krakowiec beds (KB, Fig. 6, Dyjor & Oberc, 1983;  
 470 Rasser & Harzhauser et al., 2008). In contrast, the sandy-silty sediments with lenses of brown  
 471 coal, and lignite clays of the Henryk seam (HS, Fig. 6; Dyjor 1986; Dyjor & Sadowska, 1986;  
 472 Piwocki & Ziemińska-Tworzydło, 1995) originating from ingression of the Northern Sea were  
 473 deposited in the NW part of the Fore-Sudetic block. The marine sedimentation in the PCFB  
 474 culminated around 13 Ma (Middle Serravallian; Dyjor 1981a) and terminated in the western part  
 475 around 12 Ma, and in the eastern part around 11.5 Ma (Upper Serravallian) as a hiatus due to  
 476 uplift of the PCFB and retreat of the Paratethys Sea to the SE (cf. Rasser & Harzhauser et al.,

477 2008 and others). The NW part of the Fore-Sudetic block, where the Roztoki-Mokrzyszowa  
 478 grabens (RMG, Fig. 5) are situated, was affected by the Jaworska volcanic phase, which  
 479 deposited the layer of basaltic tuff here (Birkenmajer et al., 1977). At the end of the Middle  
 480 Miocene, the stress regime switched from extensional to compressional, probably due to the  
 481 stress from the thrusting of the Outer Carpathians onto the PCFB (Badura et al., 2004; Rasser &  
 482 Harzhauser et al., 2008).

#### 483 **4.1.2 Late Miocene slow uplift/low compression and the following subsidence/extension (ca.** 484 **11–4.2 Ma)**

485 As mentioned above, the extensional regime changed throughout the WNEAF area at the  
 486 beginning of the Tortonian (Upper Miocene), when several series of compression events  
 487 occurred and caused the uplift. The strong compression event, the so-called late Styrian tectonic  
 488 phase (ca. 11.6 Ma, Fig. 6), caused the sudden uplift and the related increase in erosion, and  
 489 termination of marine sedimentation in the WNEAF area (Sissingh, 2006).

490 The late Styrian tectonic phase replaced the marine character of sedimentation by  
 491 continental sediments, the so-called Poznań formation, in the PCFB and FSB. The sedimentation  
 492 of the Poznań formation began in the Polish Lowlands basin in the Late Badenian (ca. 12-13 Ma;  
 493 Dyjor & Sadowska, 1986; Piwocki & Ziemińska-Tworzydło, 1997), and later also in the PCFB  
 494 and grabens in the FSB in the Lower Pannonian (ca. 11 Ma; Dyjor, 1981a). The lower part of the  
 495 Poznań formation, the so-called Grey Clay members (PFgy, Fig. 6), contains near seashore lake  
 496 sediments, which were interrupted by several marine incursions (Kasiński et al., 2002). This  
 497 fact indicates that the vertical uplift during the late Styrian tectonic phase was not intensive. The  
 498 uplift continued with a lower intensity during the Tortonian, when the Green Clay members  
 499 (PFGn, Fig. 6) and later Variegated Clay members (PFv, Fig. 6) of the Poznań formation were  
 500 deposited. The tectonic activity, documented by sedimentation of the Poznań formation, had a  
 501 varied character in different parts. The occurrence of sandy-gravel alluvial fans within the  
 502 Poznań formation along the southeastern margin of the FSB indicate the activity of the SMF and  
 503 low uplift of the Sudetic Mts. (Ivan, 1966; Osijuk & Piwocki, 1972; Dyjor & Kuszell, 1977). In  
 504 contrast, the maximum subsidence occurred within the FSB along the NW-SE and W-E oriented  
 505 faults (Dyjor & Oberc, 1983). The sedimentation of the Poznań formation terminated around 8  
 506 Ma, whereas in some parts, e.g. within the PCFB, it terminated as late as in the Early Pliocene  
 507 (Dyjor, 1981a).

508 The reactivation of faults due to NE-SW oriented compression since 11 Ma have also  
 509 been documented within the northern Eastern Alps Mts. (Decker et al., 1993; Peresson &  
 510 Decker, 1997b). It culminated by the retreating of the subduction boundary in the outer  
 511 Carpathians and by re-orientation of compression in an E-W direction after 9 Ma and prior to 5.3  
 512 Ma (Peresson & Decker, 1997a). In addition, Alexandrowski et al. (2005) described the E-W  
 513 oriented compression in the Carpathians as a stress field, which disrupted the Miocene sediments  
 514 at the end of the Miocene or Early Pliocene (comprehensive symbols of the paleostress marked  
 515 as d in Fig. 6).

516 The above-mentioned tectonostratigraphic situation indicates the varied tectonic activity  
 517 in different areas. The retreating of the Poznań formation basin to the N and termination of  
 518 marine incursions during the Late Miocene were probably caused by the asymmetric uplift of

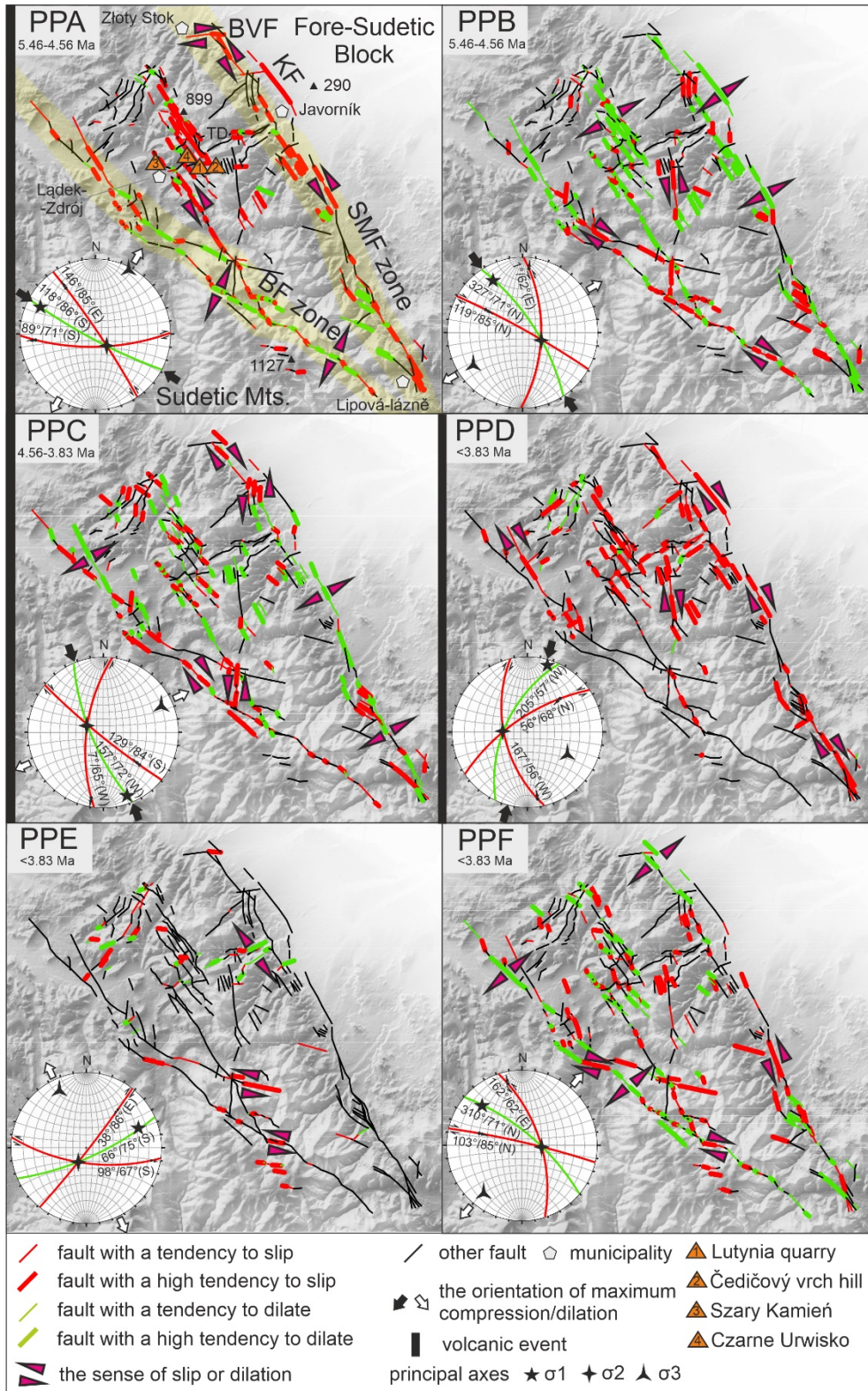
519 the Sudetic Mts. related to tilting of the Sudetic and Fore-Sudetic blocks to the N. The uplift was  
520 probably compensated by subsidence along the faults limiting the FSB to the N from the Polish  
521 Lowlands basin. The uplift must have been slow, as inferred from the mainly pelitic, sandy or  
522 coal character of the Poznań formation. The low intensive uplift of the whole of the Sudetic Mts.  
523 and the whole of the Bohemian Massif (Malkovský, 1979) continued up to the end of the  
524 Tortonian (7.2 Ma), which resulted in the complete retreat of the Paratethys and Poznań  
525 formation basins in the Polish Lowlands basin. A hiatus in the sedimentation occurred due to  
526 highly intensive erosion (Dyjor, 1981a; Dyjor & Sadowska, 1986) and was followed by  
527 sedimentation of a 5-15 m (locally up to 40 m) thick set of rough clastic material, mainly gravels  
528 and sands, the so-called Gozdnicza formation (GF, Fig. 6; Sawicki, 1997; Badura et al., 2003).  
529 The clastic material came from the uplifting of the Sudetic Mts. and the Outer Carpathians. As  
530 the GF deposited in the FSB also contains mudflow insets, the distinctly elevated Sudetic Mts.  
531 could be inferred (Ivan, 1966; 1990).

532 The intensity of the ongoing uplift in the WNEAF increased during the Messinian (Late  
533 Miocene, postdate 7.2 Ma) as the so-called Attican tectonic phase and mainly during the  
534 Zanclean (Lower Pliocene, postdating 5.3 Ma) as the so-called Rhodanian tectonic phase  
535 (Meulenkamp et al., 2000a, b; Sissingh, 2006). The main event within the WNEAF during this  
536 period was the Jura folding, which is characterized as a westward-oriented thrusting of the Jura  
537 Mts. over the eastern margin of the southernmost parts of the Rhine and Bresse grabens (Fig. 5)  
538 by 3.5 km and as a general re-emplacement of the Northern Subalpine chains. The Jura folding  
539 event was induced by an E-W to NW-SE compression within the area near the Northern  
540 Subalpine chain (Bergerat, 1987 – a, Fig. 6; Blès & Gros, 1991 – b, Fig. 6; Ziegler & Dèzes,  
541 2007) and a WNW-ESE compression in more distant areas (Ustaszewski & Schmid, 2006 – c,  
542 Fig. 6). In addition, the intensive uplift of the Sudetic Mts. resulted from the Rhodanian tectonic  
543 phase during the whole of the Lower Pliocene (Zanclean). Deposition of the GF continued on the  
544 Fore-Sudetic block (Oberc & Dyjor, 1969) and contained a thick accumulation of alluvial fans  
545 derived from the uplifting Sudetic Mts.

546 The Mio-Pliocene ~E-W compressional stress field described above perfectly matches  
547 the documented paleostress pattern PPA in orientation and timing (the Rhodanian tectonic  
548 phase). Moreover, the action of this stress field terminated after 5.46 Ma and prior to 4.56 Ma  
549 (Fig. 3). The faults striking W-E, which limit the basins (e.g. Paczków graben, Kędzierzyn  
550 graben), were activated during this time (Dyjor, 1981a), which agrees with the strike of the faults  
551 that have been recognized as potentially activated by the PPA stress field orientation. The SMF  
552 and parallel faults behaved as sinistral faults and may have been activated in the area around the  
553 town of Złoty Stok (Fig. 7). The Bílá Voda fault (BVF, Fig. 7) may have been activated as a  
554 dextral fault. In the zone of the Biala fault (BF), the fault dilation was dominant, with a small  
555 minority of the segments possibly being activated as sinistral strike slip faults. The faults in the  
556 central part of the RH Mts., where the volcanism occurred, may have also been activated as  
557 sinistral strike slip faults, but a vertical component must have also been present during the uplift  
558 of the RH Mts. According to the kinematic indicators in the volcanic rocks, the eastern blocks  
559 may have subsided against the western ones along the N-S striking faults. The presence of  
560 volcanism within the study area (Birkenmajer et al., 2002; Cajz et al., 2012) and other parts of  
561 the Bohemian Massif (Ulrych et al., 2013; Cajz et al., 2009) may indicate an episodic



562 relaxation of the stress around 5-5.5 Ma, which agrees with the episode of volcanism (Merle &  
 563 Michon, 2001) and sedimentation (Sissingh, 2001) within the WNEAF.





565 **Figure 7.** The potentially reactivated faults within the study area during action of the individual  
 566 paleostress patterns in time sequence. The main faults and the fault zones: BF zone – Biala fault  
 567 zone, BVF – Bílá Voda fault, KF – Kamenička fault, SMF zone – Sudetic Marginal fault zone.  
 568 TD – Travná intra-mountain depression.

569 The very intensive uplift and compression were disrupted within the WNEAF around 4.2  
 570 Ma and this interruption is marked by undisturbed sedimentation of Sundgau gravels (SG, Fig. 6;  
 571 Bergerat 1987; Blès & Gros, 1991; Ziegler, 1992; Meulenkamp et al., 2000a; 2000b; Dèzes et  
 572 al., 2004; Sissingh, 2006).

#### 573 **4.1.3 The Pliocene-Early Quaternary subsidence/transension and extension (4.2 – 2 Ma)**

574 At the start of this period, distinct changes in the drainage network due to tectonic  
 575 movements and opening of rift valleys occurred within the WNEAF, while fading out of the Jura  
 576 folding occurred until 3.4 Ma (Giamboni et. al., 2004). For example, around 4.2 Ma, the paleo-  
 577 Aare river was deflected from the Rhine Graben to the Bresse Graben (Fig. 5), where a new set  
 578 of fluvial Sundgau gravels was deposited (Dèzes et al., 2004). The paleostress regime changed  
 579 from reverse faulting to a strike-slip regime. The predominantly NNW-SSE oriented  
 580 compression (Ustaszewski & Schmid, 2006) caused an opening of the ENE-WSW oriented  
 581 ruptures (e, Fig. 6). During the Late Pliocene, the phase of rifting was renewed in the WNEAF,  
 582 mainly in the Rhine graben and basins in the Western Alpine foreland. The sedimentation  
 583 became confined to the accumulation of fluvio-lacustrine complexes with swamps, clastic  
 584 sequences, as well as lignite-bearing marls in isolated basins (Meulenkamp et al., 2000b;  
 585 Sissingh, 2006). Simultaneously with the rift subsidence, the uplift of the Variscan Massifs  
 586 continued and accelerated from the Late Miocene to the Early Pliocene and during the Late  
 587 Pliocene to the Quaternary (Dèzes et al., 2004; Ziegler & Dèzes, 2007). The predominantly  
 588 extensional regime began around 3.4 Ma with a maximum intensity between 3 Ma and 2.5 Ma.  
 589 Up to 2.9 Ma, fluvial Sundgau gravels (SG, Fig. 6) were depositing in the Bresse graben by the  
 590 paleo-Aare river, which was then deflected back to the Rhine graben (Fig. 5; Giamboni et. al.,  
 591 2004). Sedimentation of the Sundgau gravels terminated and a new 200 m-thick formation of  
 592 Rhine gravels (RG, Fig. 6) was deposited prior to 2.0 Ma (Dèzes et al., 2004), when the  
 593 extensional paleostress regime changed throughout the WNEAF (Sissingh, 2003). This provides  
 594 evidence of extensional subsidence and renewed rifting in the Upper and Lower Rhine grabens,  
 595 when these grabens were orthogonally extended in a NW-SE direction (Ziegler, 1992; Dèzes et  
 596 al., 2004; Ziegler & Dèzes, 2007). The dominance of the extension is also documented by syn-  
 597 sedimentary extensional faults and locally by positive flower-structures within the grabens in the  
 598 WNEAF. All of these structures resulted from an E-W to NE-SW extension (Blès & Gros, 1991  
 599 – f, Fig. 6; Dèzes et al., 2004). Ustaszewski and Schmidt (2007) interpreted these deformations  
 600 as being caused by NW-SE to N-S oriented compression (g, Fig. 6).

601 The same orientation of the transtensional stress field, ~NW-SE compression and ~NE-  
 602 SW extension, was observed within the study area as the paleostress patterns PPB and PPC in the  
 603 period between 4.56 and 3.83 Ma. Both paleostress patterns probably represent one paleostress  
 604 event with transtensional parameters changing over time due to the similar orientation of the  $\sigma_3$   
 605 axis. The NE-SW extension resulted in enlarging of the FSB and the Intra-Sudetic basins (e.g.  
 606 Upper Nysa Kłodzka graben, UNKG, Fig. 1). The WNW-ESE to NW-SE striking faults were  
 607 activated with a 70 m vertical throw and created the eastern shoulder of the UNKG (Badura &

608 Rauch, 2014). The WNW-ESE to NW-SE faults may have also been activated as dextral (during  
609 the PPB and PPC) and the N-S faults may have been activated as sinistral (during the PPB and  
610 PPC). The SMF zone may have tended to dilate, with only some N-S oriented segments near the  
611 town of Javorník having been activated as sinistral strike slip faults (Fig. 7). The straight trace of  
612 the SMF may have been disrupted and split by ~N-S striking faults into zigzagging segments.  
613 According to kinematic indicators in the volcanic rocks, the northern blocks mainly subsided  
614 (during the PPB and PPC) against the southern ones along the ENE-WSW to WNW-ESE  
615 striking subvertical faults (see the block diagrams in Fig. 4). These movements are reflected in  
616 the vertical contrast between the Sudetic Mts. and the Fore-Sudetic block. The BF zone may  
617 have been more active in this period. Most of the segments may have been activated as dextral  
618 strike slip faults with the expected vertical component in the range of tens of meters. The faults  
619 in the central part of the RH Mts. may have dilated, which may have corresponded to relaxation  
620 after the previous mountain ridge uplift. This transtension regime was probably terminated after  
621 the higher volcanic activity in the area of the RH Mts. and elsewhere within the Bohemian  
622 Massif (e.g. Adamovič & Coubal, 1999; Ulrych et al., 2013; Merle & Michon, 2001) around 3.83  
623 Ma.

624 The Bohemian Massif underwent stagnation of the uplift or even weak subsidence during  
625 the Late Pliocene to Early Pleistocene, which is evident by the accumulation of lacustrine  
626 sediments mainly in the Cheb basin (CHB), Southern Bohemian basins (SBB) and Upper  
627 Morava graben (UMG). In the CHB, the lacustrine pelitic Vonšov member (VM, Fig. 6) as a part  
628 of the Vildštejn formation aged 4.7 Ma – 1.4 Ma (after Bucha et al., 1990; Upper Pliocene to  
629 Quaternary age after Pešek, ed., 2010) was discordantly deposited on the Cypris formation after  
630 a 12 Ma-long hiatus. The sedimentation in the Cheb and Domažlice basins (DB, Fig. 5) was  
631 caused by relative subsidence of the western block along the NNW-SSE oriented Mariánské  
632 lázně fault under a NE-SW oriented extensional regime (h, Fig. 6; Špičáková et al., 2000). In the  
633 nearby Most basin (MB, Fig. 5), the Pliocene Vysočany river terrace was faulted probably due to  
634 an NNE-SSW oriented extension (Coubal & Adamovič, 2000 – i, Fig. 6). Similarly, lacustrine  
635 sediments of the Ledenice formation (LF, Fig. 6) were deposited in the SBB and in the UMG, the  
636 Upper Pliocene to Quaternary fluvial sediments known as the Křelov formation (KF, Fig. 6)  
637 occur. The reactivation and subsidence along the NNW-SSE oriented faults caused by the ENE-  
638 WSW oriented extension are mentioned in the UMG in Růžička (2014; j, Fig. 6). Sedimentation  
639 of the Gozdnica formation continued within the area of the FSB (Dyjor, 1981a). The fluvial  
640 gravels with a kaolinic matrix, deposited in deep channels eroded in the upper part of the GF, the  
641 so-called pre-glacial formation, white gravels or the Ziebice group (ZG, Fig. 6; e.g. Przybylski et  
642 al., 1998; Dyjor, 1966; Czerwonka & Kryszkowski, 2001), have been described as being a result  
643 of Late Pliocene erosion (Walczak, 1954; 1970). The increase in bedrock erosion and common  
644 saprolite redeposition was probably caused by an increase in tectonic activity (Czerwonka &  
645 Kryszkowski, 2001) and is related also to progressive cooling of the climate (Badura et al., 2004)  
646 during the Late Pliocene and Early Pleistocene. The ZF was derived from the Sudetic Mts. being  
647 uplifted and is related to a higher erosion rate in the area of the FSB during the Middle Zanclean  
648 and Early Gelasian (Czerwonka & Kryszkowski, 2001). According to Badura et al. (2003), the  
649 pre-glacial formation originated as Pliocene gravels redeposited by sub-glacial rivers of a Mezo-  
650 Pleistocene age. In comparison to other areas of the WNEAF, the character of the ZG sediments

651 is similar to the character of the Sangau and Rhine gravels within the URG, where the origin of  
652 the sediments is clearly tectonic.

653 The above- mentioned short period of uplift during the Late Zanclean may correspond to  
654 the newly discovered event of the NNE-SSW compression described in this paper, which is  
655 represented by paleostress pattern PPD and which interrupted the period of extensional tectonic  
656 regime that lasted since the Early Pliocene. This phase is characterized as a NE-SW dominant  
657 compression. The SMF may have behaved as a dextral fault with a vertical normal component,  
658 mainly between Javorník and Złoty Stok. The BF was probably not active during this tectonic  
659 phase. The faults in the central part of the RH Mts. may have been activated as dextral faults  
660 with a vertical component (Fig. 7). According to the kinematic records in volcanic rocks, this  
661 stress regime produced the horst-like structures along the NNW-SSE and NE-SW faults (see the  
662 block diagram in Fig. 4). The subsidence of the northern and southern blocks was also suggested  
663 by Skácel and Vosska (1959). This compressional event may have represented the stress  
664 transmission from the Carpathians as described in Stemberk Jr. et al. (2019).

665 The newly discovered paleostress pattern PPE is characterized as a distinct NNW-SSE  
666 oriented extension with a near normal fault regime. This hitherto unknown paleostress pattern  
667 indicates a different orientation of extension during the Piacenzian than other authors mentioned.  
668 Paleostress pattern PPE may not have affected some of the faults in the study area. No segments  
669 of the SMF zone were probably activated, only several ~W-E segments of the BF may have been  
670 activated as sinistral faults. The ENE-WSW faults, which limit the Travná intra-mountain  
671 depression (Ivan, 1966 and Stemberk Jr. et al., 2019; TD in Fig. 7) may have been dilated and  
672 created or at least morphologically accentuated this depression. The Travná depression has a  
673 complicated block-like structure in the longitudinal as well as cross-sectional profile, which  
674 agrees with the kinematic pattern derived from the data on volcanic rocks (see the block diagram  
675 of PPE in Fig. 4).

676 The above-mentioned ENE-WSW to NE-SW oriented extensional regime may have  
677 caused similar tectonostratigraphic evolution and deformations within the whole WNEAF and  
678 Bohemian Massif. Paleostress pattern PPF agrees with the above-mentioned extensional regime  
679 during this period. Parameters of the paleostress tensor indicate the distinct extension with a  
680 near-normal fault regime (Tab. 1) within the study area. The action of paleostress pattern PPF  
681 postdates 3.83 Ma. Paleostress pattern PPF may have affected mainly the NNW-SSE oriented  
682 faults by a sinistral sense of slip and WNW-ESE striking faults by a dextral sense of slip. The BF  
683 zone may have tended to dilate, only several short segments may have been activated as dextral  
684 faults. Within the SMF zone, several segments striking NNW-SSE may have been activated as  
685 sinistral. The straight line of the SMF may have been disrupted by the NE-SW oriented faults  
686 into zigzagging segments, which are recognizable in the relief until today. The block diagram of  
687 PPF in Fig. 4 shows the subsidence of the northeastern blocks. During this stress pattern, the  
688 northern mountain front of the RH Mts. may have been accentuated due to movement on the  
689 SMF.

#### 690 **4.1.4 Quaternary compressional events and uplift of massifs (ca. 2 Ma – to-date)**

691 The regional hiatus is documented at the end of the Gelasian (about 1.8 - 2 Ma) and is  
692 related to renewed regional uplift, termination of sedimentation in the WNEAF and Bohemian

693 Massif, and to rapid reconfiguration of paleohydrography throughout the WNEAF (Sissingh,  
694 2003). This distinct tectonic event corresponds to build-up of the present-day NW-SE oriented  
695 compressional stress field and is the so-called Wallachian tectonic phase. The Pliocene Sundgau  
696 gravels along the Jura Mts. front were probably folded by the same or a similar compressional  
697 impulse, postdating 2.9 Ma (Giamboni et. al., 2004). The results of the paleostress analyses  
698 indicate the N-S to NW-SE oriented compression (Ustaszewski & Schmid, 2006 – k, Fig. 6). The  
699 tectonic event that affected the whole of the Alpine and Carpathian forelands during this period  
700 is called the Wallachian phase (Hippolyte & Sandulescu, 1996).

701 Within the Bohemian Massif, the lacustrine sedimentation of the Gelasian (Lower  
702 Pleistocene) and Calabrian (Middle Pleistocene) sediments was replaced by locally discordantly  
703 accumulated chaotic fluvial sediments and enhanced erosion during the Early Quaternary as a  
704 response to the uplift (Malkovský, 1979). In the CHB, the sedimentation of the lacustrine  
705 Vonšov Member was replaced by heterogenous sandy gravels of the Nová Ves formation (NV,  
706 Fig. 6; Pešek, ed., 2010). In the SBB, the sedimentation of the lacustrine Ledenice formation was  
707 replaced by sandy gravels of the Moldavite Gravels (MG, Fig. 6). The uplift of the Šumava Mts.  
708 and Český les Mts. caused the deflection of the originally southward-flowing rivers to the north  
709 (Pešek, ed., 2010). In the UMG, the down-cutting erosion affected the Křelov formation,  
710 probably as a result of the Bohemian Massif uplift (Růžička, 2014). In the area of the FSB, an  
711 interruption of the sedimentation (hiatus) occurred at the beginning of the Early Pleistocene  
712 (Czerwonka & Krzyszkowski, 2001). The Sudetic Mts. were uplifted by about 60-300 m in  
713 different parts and also the FSB was uplifted by about 40-80 m (Przybylski et al., 1998) due to  
714 stress field changes and caused the reconfiguration of the drainage network and an increase in  
715 erosion (Ivan, 1966).

716 This stress pattern during the last period is an NW-SE oriented compression (l, Fig. 6),  
717 which was previously documented by Adamovič and Coubal (1999), Coubal et al. (2015; marked  
718 as paleostress pattern  $\delta$ ). The action of this stress field, which caused the uplift of the WNEAF  
719 and Bohemian Massif, was probably interrupted by several episodes of stress relaxation. This  
720 interruption is supported by young volcanism between 1.0 and 1.8 Ma (Cajz et al., 2012; Ulrych  
721 et al., 2013). Despite the stress relaxation, the continuation of episodic uplift is documented by  
722 the start of deep erosion and river terrace development around 0.7-0.8 Ma in the Variscan  
723 massifs (Ziegler & Dèzes, 2007). Moreover, the stress field has been influenced and modified by  
724 loading of the continental ice-sheet, which covered the FSB. The Middle and Late Pleistocene  
725 tectonic activity of the SMF, which was enhanced by post-glacial rebound, was suggested by  
726 faulted river terraces in the Sudetic Mts., showing 5-20 m vertical offsets in their longitudinal  
727 profiles (Krzyszkowski & Pijet 1993). The affected fluvial terraces in the FSB showed  
728 diminishing uplift intensity from the Middle Pleistocene to the Late Pleistocene based on  
729 decreasing vertical offsets of the terraces from ~20 to 3 m (Štěpančíková et al., 2008). Similar  
730 values of post-glacial uplift (post-Saalian/post-130 ka in the study area) of 20-35 m, with  
731 decreasing tendency (2-5 m in the Late Pleistocene), are reported also from the Sudetic Mts.  
732 (Badura et al., 2004), while the estimate of their total uplift along the SMF during the Middle and  
733 Late Pleistocene is 20-30 m up to 60-80 m (Krzyszkowski & Pijet 1993; Dyjor, 1981b;  
734 Przybylski, 1998; Badura & Przybylski, 1998). The decrease in the uplift intensity may have  
735 been ascribed to ice-sheet loading. Late Pleistocene activity of the SMF was also directly  
736 documented in paleoseismological trenches excavated between Złoty Stok and Javorník. The  
737 alluvial fan apex at one of the sites is truncated by the SMF and has a left-laterally offset of 30-

738 45 m from the feeder channel as a response to ice-sheet loading during the Last Glacial  
739 Maximum (~20ka; Štěpančíková & Stemberk Jr., 2016).

740 Based on the World Stress Map (Heidbach et al., 2016), two distinct provinces of the  
741 present-day stress field were delimited nearby the study area. The first province is the Western  
742 European Stress Domain comprising the W and NW parts of the Central European Platform,  
743 including the Bohemian Massif. The domain is influenced by sub-horizontal stress of NW to  
744 NNW orientation caused by the push resulting from the North Atlantic Ridge spreading (Müller  
745 et al., 1992; Jarosiński et al., 2006). The stress with dominant compression was determined in the  
746 western part of the Bohemian Massif by Peška (1992; m, Fig. 6) based on borehole breakouts, by  
747 Vavryčuk et al. (2012) based on earthquake focal mechanisms and in the eastern part by Havíř  
748 (2004; q, Fig. 6) and with dominant extension by Špaček et al. (2015; n, Fig. 6) based on  
749 earthquake focal mechanisms. The second province is represented by the Fore-Carpathian stress  
750 domain, where the NNE-SSW to N-S oriented compression is present. The stress field is  
751 generated by the tectonic push of the African plate transmitted into the foreland by ALCAPA  
752 microplate. The different stress orientations in the upper (p, Fig. 6) and deeper parts of the  
753 Earth's crust (o, Fig. 6) separated by a décollement layer in the Jura Mts., were presented by  
754 Ustaszewski and Schmidt (2006). The present-day switching of the stress pulses of both of the  
755 stress field orientations was recorded by extensometers monitoring micro-displacements on the  
756 faults in the RH Mts. between 2014 and 2017 (Stemberk Jr. et al., 2019 – r, Fig. 6).

757 Nevertheless, the records of the last stress patterns have not been noticed in brittle  
758 tectonics of the volcanic rocks in the study area. This is probably due to the fact that the volcanic  
759 rocks reached positions near the surface, where the sub-horizontal and also normal stress field  
760 cannot act due to relief geometry. The Quaternary uplift and the resulting erosion later  
761 completely exposed the outcrops on the surface as elevations. The volcanic rock columns have  
762 been dilating and weathered, fissures have been opened or widened due to climatic causes and  
763 are no longer in direct contact, which would enable the striation process.

## 764 **5 Conclusions**

765 A study of paleostress markers, such as striae on slickensides, in dated volcanic rocks in  
766 the Rychlebské hory Mts. resulted in the differentiation of six paleostress patterns (regimes)  
767 since the Late Miocene up to ca. 2 Ma. Each paleostress pattern is characterized by the  
768 orientation of the principal parameters. These paleostress patterns were discussed in the light of  
769 other known paleostress patterns within the surrounding regions of the Sudetic Mts., Fore-  
770 Sudetic block and the European Alpine foreland. The comparison rules out the possible influence  
771 of thermic changes and a possible striae origin due to the cooling down of the volcanic rocks or  
772 ongoing quarry activity. Moreover, a comparison of the tectonostratigraphic relations of the  
773 sedimentary basins in the WNEAF and Polish Lowlands basin discovered the relation between  
774 periods with dominant subsidence, when the extension stress regime predominated, in contrast to  
775 periods with dominant uplift, when the compressional stress regime predominated. This new  
776 approach allows more accurate and detailed time constraints of the action of the paleostress  
777 patterns. The results show switching of tectonic phases with dominant compression, transtension  
778 or extension. The following paleostress patterns were identified.

- 779 - PPA with dominant WNW-ESE compression between 5.46 Ma and 4.56 Ma, which  
780 corresponds to the end of the W-E Miocene stress field.
- 781 - PPB transtensional regime with dominant NE-SW extension between 5.46. and 4.56  
782 Ma.
- 783 - PPC transtensional regime with a NE-SW extension character between 4.56 Ma and  
784 3.83 Ma.
- 785 - PPD with dominant NE-SW compression postdating 3.83 Ma.
- 786 - PPE with dominant NNW-SSE extension postdating 3.83 Ma
- 787 - PPF with dominant ENE-WSW extension postdating 3.83 Ma

788 Because the stress conditions are crucial for the evolution of the Earth's surface, the  
789 activity and expected behavior of the fault systems within the study area during the individual  
790 periods of the paleostress patterns were suggested as presented in Fig. 7. This figure indicates the  
791 episodic re-activation of several segments of the Sudetic Marginal fault and Bělský fault. The  
792 results are given in a wide context by other authors, who deal with the evolution of the Sudetic  
793 Mts., the Fore-Sudetic block and also in the whole of the European Alpine foreland.

794 The newly discovered paleostress pattern PPD may reveal a hitherto unknown short  
795 period of uplift during the Late Zanclean (postdating 3.83 Ma), which caused erosion of the  
796 upper part of the Gozdnic formation. Moreover, the sedimentation was restored within the  
797 Bohemian Massif basins after this short period. Paleostress pattern PPE was also discovered,  
798 which is characterized as a distinct NNW-SSE oriented extension with a near normal fault  
799 regime. This until now unknown paleostress pattern indicates a different orientation of the  
800 extension during the Piacenzian age. Other determined paleostress patterns are similar to the  
801 known stress regimes within the WNEAF and Polish Carpathian Foredeep basin, which indicate  
802 the supra-regional tectonic origin.

### 803 **Acknowledgments**

804 This research was carried out in the framework of the Charles University in Prague,  
805 Czechia, supported by project GAUK862213 - Multidisciplinary geophysical survey in  
806 investigation of landforms, and within long-term conceptual development research organization  
807 of the Czech Academy of Sciences RVO: 67985891. Some parts were conducted thanks to  
808 support of research program KONTAKT II by Ministry of Education, Youth and Sports of the  
809 Czechia as project LH12078 - Assessment of Tectonic Movements on Active faults, the project



810 no. LTV20022 in research program INTER-EXCELLENCE and the project CzechGeo/EPOS -  
811 Sci CZ.02.1.01/0.0/0.0/16\_013/0001800.

812 Datasets for this research are available in this citation references: Stemberk, J. jr. (2020)  
813 with license CC BY 4.0.

## 814 **References**

- 815 Adamovič, J., & Coubal, M. (1999). Intrusive geometries and Cenozoic stress history of the northern part of the  
816 Bohemian Massif. *Geolines*, 9, 5-14.  
817
- 818 Aleksandrowski, P., Kryza, R., Mazur, S., Pin, C., & Zalasiewicz, J. A. (2000). The Polish Sudetes: Caledonian or  
819 Variscan?. *Transactions of the Royal Society, Edinburgh*, 90, 127–146. <http://doi.org/10.1017/S0263593300007197>  
820
- 821 Aleksandrowski, P., & Mazur, S. (2002). Collage tectonics in the northeasternmost part of the Variscan Belt: the  
822 Sudetes, Bohemian Massif. In Winchester, J., Pharaoh, T., & Verniers, J. (Eds.), *Palaeozoic Amalgamation of*  
823 *Central Europe. Geological Society, London, Special Publications*, 201, 237–277.  
824 <http://doi.org/10.1144/GSL.SP.2002.201.01.12>  
825
- 826 Alexandrowski, P., Krzywiec, P., Ryzner-Siupik, B., Papiernik, B., Siupik, J., Mastalerz, K., et al. (2005). The  
827 Anatomy of Strike-Slip Gas-Bearing Structure of Ryszkowa Wola (Carpathian Foreland Basin, SW Poland) as  
828 Revealed by 3D Seismics: a Product of Late Sarmatian-Pliocene (?) Episode of E–W Directed Tectonic  
829 Compression. *Geolines*, 19, 16-17.  
830
- 831 Allmendinger, R. W., Cardozo, N. C., & Fisher, D. (2012). *Structural Geology Algorithms: Vectors & Tensors.*  
832 *Cambridge University Press*, 289 pp. <http://doi.org/10.1017/CBO9780511920202>  
833
- 834 Angelier, J. (1989). From orientation to magnitudes in paleostress determination using fault slip data. *Journal of*  
835 *Structure Geology*, 11, 37-50. [https://doi.org/10.1016/0191-8141\(89\)90034-5](https://doi.org/10.1016/0191-8141(89)90034-5)  
836
- 837 Angelier, J. (1994). Inversion of brittle tectonic data in order to determine stress tensor – faults, non-faults and  
838 pressure tension structures. *Bulletin de la Societe Geologique de France*, 165(3), 211-220.  
839
- 840 Angelier J., Tarantola A., Valette, B., & Manoussis, S. (1982). Inversion of field data in fault tectonics to obtain the  
841 regional stress - 1. Single phase fault populations: a new method of computing the stress tensor. *Geophys. J. R. astr.*  
842 *Soc.*, 69, 607-621. <http://doi.org/10.1111/j.1365-246X.1982.tb02766.x>  
843
- 844 Badura, J., & Przybylski, B. (1998). Zasięgi lądolodów plejstocenijskich i deglacja obszaru między Sudetami a  
845 Wałem Śląskim (Extent of the Pleistocene ice sheets and deglaciation between the Sudeten and the Silesian  
846 Rampart), *Biuletyn Państwowego Instytutu Geologicznego (Journal of the Polish national geological institute)*, 385,  
847 9-27. (in Polish with English abstract)  
848
- 849 Badura, J., Przybylski, B., & Zuchiewicz, W. (2004). Cainozoic evolution of Lower Silesia, SW Poland: A new  
850 interpretation in the light of sub-Cainozoic and sub-Quaternary topography. *Acta Geodyn. Geomater*, 1 (135), 7-29.  
851
- 852 Badura, J., Zuchiewicz, W., Górecki, A., Sroka, W., Przybylski, B., & Źyszkowska, M. (2003). Morphotectonic  
853 properties of the Sudetic Marginal Fault, SW Poland. *Acta Montana, A*, 24(131), 21-49.  
854
- 855 Badura, J., Zuchiewicz, W., Štěpančíková, P., Przybylski, B., Kontny, B., & Cacoń, S. (2007). The Sudetic Marginal  
856 Fault: A young morphotectonic feature at the NE margin of the Bohemian Massif, Central Europe. *Acta Geodyn.*  
857 *Geomater.*, 4(148), 7-29.  
858
- 859 Badura, J., & Rauch, M. (2014). Tectonics of the Upper Nysa Kłodzka Graben, the Sudetes. *Geologia Sudetica*, 42,  
860 137–148.  
861

- 862 Berger, F. (1932). Die Alterstellung des Basaltes vom Grauer Stein bei Landeck, Grafschaft Glatz (The position of  
863 volcanics of the Szary Kamień by Łądek Zdrój, county Glatz). *Entralblatt für Min., B*, 545-553.  
864
- 865 Bergerat, F. (1987). Stress field in the European platform at the time of Africa–Eurasia collision. *Tectonics*, 6, 99–  
866 132. <http://doi.org/10.1029/TC006i002p00099>  
867
- 868 Birkenmajer, K., Jeleńska, M., Kądziałko-Hofmokl, M., & Kruczyk, J. (1977). Age of deep-seated fracture zones in  
869 Lower Silesia (Poland), based on K-Ar and paleomagnetic dating of Tertiary basalts. *Annales de la Société*  
870 *Géologique de Pologne*, 47(4), 545-552.  
871
- 872 Birkenmajer, K., Pécskay, Z., Grabowski, J., Lorenc, M. W., & Zagożdżon, P. (2002). Radiometric dating of the  
873 Tertiary volcanics in Lower Silesia, Poland. II. K-Ar and paleomagnetic data from Neogene basanites near Łądek  
874 Zdrój, Sudetes Mts.. *Annales Societatis Geologorum Poloniae*, 72, 119-129.  
875
- 876 Blès, J.-L., & Gros, Y. (1991). Stress field changes in the Rhone Valley from the Miocene to the present.  
877 *Tectonophysics*, 194, 265–277. [https://doi.org/10.1016/0040-1951\(91\)90264-S](https://doi.org/10.1016/0040-1951(91)90264-S)  
878
- 879 Bucha, V., Horáček, J., & Malkovský, M. (1990). Palaeomagnetic stratigraphy of the Tertiary of the Cheb Basin (W  
880 Bohemia). *Věstník Ústředního ústavu geologického (Journal of Geological institute)*, 65(5), 267-278. (in Czech)  
881
- 882 Buday, T., Ďurica, D., Opletal, M., & Šebesta, J. (1997). Význam bělského a klepáčovského zlomového systému a  
883 jeho pokračování do Karpat (The importance of the Bělá and Klepáčov fault system and their continuation to  
884 Carpathians). *URGP (Journal of Coal, ore and geological investigations)*, 9, 275-281. (in Czech)  
885
- 886 Cajz, V., Rapprich, V., Schnabl, P., & Pécskay, Z. (2009). Návrh litostratigrafie neovulkanitů východočeské oblasti  
887 (A proposal on lithostratigraphy of Cenozoic volcanic rocks in Eastern Bohemia). *Geoscience Research Reports for*  
888 *2008*, 9-14. (in Czech)  
889
- 890 Cajz, V., Schnabl, P., Pécskay, Z., Skácelová, Z., Venhodová, D., Šlechta, S., & Čížková, K. (2012). Chronological  
891 implications of the paleomagnetic record of the Late Cenozoic volcanic activity along the Moravia-Silesia border  
892 (NE Bohemian Massif). *Geologica Carpathica*, 63(5), 423-435. <http://doi.org/10.2478/v10096-012-0033-3>  
893
- 894 Coubal, M., & Adamovič, J. (2000). Youngest tectonic activity on faults in the SW part of the Most Basin. *Geolines*,  
895 *10*, 15-17.  
896
- 897 Coubal, M., Málek, J., Adamovič, J., & Štěpančíková, P. (2015). Late Cretaceous and Cenozoic dynamics of the  
898 Bohemian Massif inferred from the paleostress history of the Lusatian Fault Belt. *Journal of Geodynamics*, 87, 26-  
899 49. <http://doi.org/10.1016/j.jog.2015.02.006>  
900
- 901 Cwojdzinski, S. (1977). Szczegółowa Mapa Geologiczna Sudetów, 902C-Trzebieszowice (Geological maps of  
902 Sudetes, sheet 902C-Trzebieszowice). *Institut Geologiczny (Polish Geological Institute)*.  
903
- 904 Cwojdzinski, S. (1981). Szczegółowa Mapa Geologiczna Sudetów, 934A-Stronie Śląskie (Geological maps of  
905 Sudetes, sheet 934A-Stronie Śląskie). *Institut Geologiczny (Polish Geological Institute)*.  
906
- 907 Cymerman, Z., & Cwojdzinski, S. (1984). Szczegółowa Mapa Geologiczna Sudetów, 934B-Strachocin, Bielice  
908 (Geological maps of Sudetes, sheet 934B-Strachocin, Bielice). *Institut Geologiczny (Polish Geological Institute)*.  
909
- 910 Czerwonka, J. A., & Krzyszkowski, D. (2001). Preglacial (Pliocene – Early Middle Pleistocene) deposits in  
911 Southwestern Poland: lithostratigraphy and reconstruction of drainage pattern. In: Krzyszkowski, D. (Ed.), Late  
912 Cainozoic Stratigraphy and Palaeogeography of the Sudetic Foreland. *Wind, J. Wojewoda*, 147-195.  
913
- 914 Danišik, M., Štěpančíková, P., & Evans, N. J. (2012). Constraining long-term denudation and faulting history in  
915 intraplate regions by multisystem thermochronology: An example of the Sudetic Marginal Fault (Bohemian Massif,  
916 central Europe). *Tectonics*, 31. <http://doi.org/10.1029/2011TC003012>

- 917 Decker, K., Meschede, M., & Ring, U. (1993). Fault slip analysis along the northern margin of the Eastern Alps  
 918 (Molasse, Helvetic nappes, North and South Penninic flysch, and the Northern Calcareous Alps). *Tectonophysics*,  
 919 223(3-4), 291-312. [http://doi.org/10.1016/0040-1951\(93\)90142-7](http://doi.org/10.1016/0040-1951(93)90142-7)  
 920
- 921 Dèzes, P., Schmid, S. M., & Ziegler, P. A. (2004). Evolution of the European Cenozoic Rift System: interaction of  
 922 the Alpine and Pyrenean orogens with their foreland lithosphere. *Tectonophysics*, 389, 1–33,  
 923 <http://doi.org/10.1016/j.tecto.2004.06.011>  
 924
- 925 Don, J., Skácel, J., & Gotowała, R. (2003). The boundary zone of the East and West Sudetes on the 1:50 000 scale  
 926 geological map of the Velké Vrbno, Staré Město and Šniežnik Metamorphic Units. *Geologia Sudetica*, 35, 25–59.  
 927
- 928 Dyjor, S. (1981a): Ewolucja trzeciorzędowych przedgórskich rowów tektonicznych centralnych i wschodnich  
 929 Sudetów (The evolution of the Tertiary tectonics in central and eastern part of the Sudetes). In Kwiecień, L. (Ed.),  
 930 III. Sympozjum - Współczesne i neotektoniczne ruchy skorupy ziemskiej w Polsce (III. Symposium – Present-day  
 931 and neotectonic movements of the earth's crust in Poland). *Ossolineum, Wrocław*, 155–181. (in Polish with English  
 932 summary)  
 933
- 934 Dyjor, S. (1981b). Problemy wieku dolnej granicy i fazy ruchów neotektonicznych w południowo-zachodniej Polsce  
 935 (The age of the lower limit and phases of the neotectonic movements in southwestern Poland). In Kwiecień, L.  
 936 (Ed.), III. Sympozjum - Współczesne i neotektoniczne ruchy skorupy ziemskiej w Polsce (III. Symposium –  
 937 Present-day and neotectonic movements of the earth's crust in Poland). *Ossolineum, Wrocław*, 25-41. (in Polish with  
 938 English summary)  
 939
- 940 Dyjor, S. (1986). Evolution of sedimentation and paleogeography of near-frontier areas of the Silesian Part of the  
 941 Paratethys and Tertiary Polish-German Basin. *Kwartalnik AGH, Geol.*, 12(3), 7-24.  
 942
- 943 Dyjor, S. (1966). Wiek serii białych żwirów i glin kaolinowych w zachodniej części przedpola Sudetów, (The age of  
 944 the white gravels and kaolinic soils in the western part of the Sudetic Foreland). *Prz. Geol.*, 14, 478-479. (in Polish)  
 945
- 946 Dyjor, S., & Sadowska, A. (1986). An attempt of correlation of stratigraphic and lithostratigraphic units of Tertiary  
 947 in western part of Polish Lowlands and Silesian part of Paratethys (IGCP 25). *Przegląd Geologiczny*, 7, 380–386.  
 948
- 949 Dyjor, S., & Kuszel, T. (1977). Neogeneńska i czwartorzędowa ewolucja rowu tektonicznego Roztoki-Mokrzyszowa  
 950 (Neogene and Quaternary evolution of the Roztoki-Mokrzyszow tectonic grabens). *Geologia Sudetica*, 13(3).  
 951
- 952 Dyjor, S., & Oberc, J. (1983). Recent crustal movements in SW Poland causing possible damage in mines and in  
 953 industrial objects, Materiały III Krajowego Sympozjum "Współczesne i neotektoniczne ruchy skorupy ziemskiej w  
 954 Polsce". *Ossolineum, Wrocław*, 4, 7-23. (in Polish, with English summary)  
 955
- 956 Farr, T. G., (Eds.) (2007). The Shuttle Radar Topography Mission. *Rev. Geophys.*, 45, RG2004, Last access: 12 Nov  
 957 2018. <https://www2.jpl.nasa.gov/srtm>, <http://doi.org/10.1029/2005RG000183>  
 958
- 959 Fediuk, F., & Fediuková, E. (1989). Ultramafické nodule severomoravských bazaltoidů (Ultramafic nodules in  
 960 basalts from northern Moravia, Czechoslovakia). *Sbor. Geol. Věd – Geologie (Journal of Geological Sciences –*  
 961 *Geology)*, 44, 9-49.  
 962
- 963 Fossen, H. (2010). Structure Geology. *Cambridge University Press, New York*, 463 pp.  
 964 <http://doi.org/10.1017/CBO9780511777806>  
 965
- 966 Franke, W., & Żelaźniewicz, A. (2000). The eastern termination of the Variscides: terrane correlation and kinematic  
 967 evolution. In Franke, W., Haak, V., Oncken, O., & Tanner, D. (Eds.), *Orogenic Processes: Quantification and*  
 968 *Modelling in the Variscan Belt. Geological Society, London, Special Publications*, 179, 63–86.  
 969 <http://doi.org/10.1144/GSL.SP.2000.179.01.06>  
 970
- 971 Gabriel, M., Gabrielová, N., Hokr, Z., Knobloch, E., & Kvaček, Z. (1982). Miocén ve vrtu Vidnava Z-1 (Miocene  
 972 formation in borehole by Vidnava town). *Journal of Geological Sciences, part Geology*, 36, 115-137. (in Czech)

- 973  
974 Giamboni, M., Ustaszewski, K., Schmid, S. M., Schumacher, M. E., & Wetzel, A. (2004). Plio-Pleistocene  
975 transpressional reactivation of Paleozoic and Paleogene structures in the Rhine-Bresse transform zone (northern  
976 Switzerland and eastern France). *Int J Earth Sci (Geol. Rundsch)*, 93, 207–223. <http://doi.org/10.1007/s00531-003-0375-2>  
977  
978  
979 Gierwielanic, J. (1968). Szczegółowa Mapa Geologiczna Sudetów, 902D-Lądek Zdrój (Geological maps of Sudetes,  
980 sheet 902D-Lądek Zdrój). *Institut Geologiczny (Polish Geological Institute)*.  
981  
982 Guterch, B., & Lewandowska-Marciniak, H. (2002). Seismicity and seismic hazard in Poland. *Folia Quaternaria*,  
983 73, 85-99.  
984  
985 Havíř, J. (2002). Variscan and Post-Variscan Paleostresses on the Southeastern Margin of the Nížký Jeseník Region  
986 (Czech Republic). *Geolines*, 14, 33-34.  
987  
988 Havíř, J. (2004). Orientation of recent principal stress axes in the Jeseníky region. *Acta Geodyn. Geomater.*, 1(135),  
989 49-57.  
990  
991 Heidbach, O., Rajabi, M., Reiter, K., Ziegler, M., & WSM Team (2016). World Stress Map Database Release 2016.  
992 *GFZ Data Services*. <http://doi.org/10.5880/WSM.2016.001>  
993  
994 Hippolyte, J. C., Bellier, O., & Espurt, N. (2012). Quaternary deformation and stress perturbations along the Digne  
995 thrust front, Southwestern Alps. *Comptes Rendus Geoscience*, 344(3-4), 205-213.  
996 <http://doi.org/10.1016/j.crte.2012.03.002>  
997  
998 Hippolyte, J. C., & Sandulescu, M. (1996). Paleostress characterization of the "Wallachian phase" in its type area  
999 (southeastern Carpathians, Romania). *Tectonophysics*, 263(1-4), 235-248. [http://doi.org/10.1016/S0040-1951\(96\)00041-8](http://doi.org/10.1016/S0040-1951(96)00041-8)  
1000  
1001  
1002 Hynie, O. (1963). Minerální vody (Mineral waters). *Nakl. Českoslov. Akad. Věd (Czechoslovak Academy of Sciences press)*, 797 pp. (in Czech)  
1003  
1004  
1005 Ivan, A. (1990). K charakteru neotektonických pohybů a vývoji reliéfu v oblasti Hrubého Jeseníku a východní části  
1006 Orlických hor (The character of the neotectonic movements and relief evolution in Hrubý Jeseník Mts. and eastern  
1007 part of the Orlické hory Mts.). *Čas. Slez. Muz. (Journal of the Silesian Museum)*, A, 39, 277-281.  
1008  
1009 Ivan, A. (1966). Geomorfologické poměry severozápadní části Rychlebských hor, Kandidátská práce  
1010 (Geomorphological conditions of NW part of the Rychlebské hory Mts., Ph.D. theses). *Geological Institute of the*  
1011 *Czechoslovak Academy of Sciences, Brno*, 120 pp. (in Czech)  
1012  
1013 Ivan, A. (1997). Topography of the Marginal Sudetic Fault in the Rychlebské hory Mts. and geomorphological  
1014 aspects of epiplatform orogenesis in the NE part of Bohemian Massif. *Moravian Geographic Reports*, 5, 3-17.  
1015  
1016 Jarosiński, M., Beekman, F., Bada, G., & Cloetingh, S. (2006). Redistribution of recent collision push and ridge  
1017 push in Central Europe: Insights from FEM modelling. *Geophys. J. Int.*, 167, 860–880.  
1018 <http://doi.org/10.1111/j.1365-246X.2006.02979.x>  
1019  
1020 Jelínek, J. (2008). Morphotectonic analysis of the digital relief model – a suitable means of searching for zones of  
1021 rock mass brittle failure. *GeoScience Engineering*, 54(3), 1-13.  
1022  
1023 Kasiński, J. R., Czapowski, G., & Gąsiewicz, A. (2002). Marine-influenced and continental settings of the Poznań  
1024 Formation (Upper Neogene, Central and SW Poland). In Gürs, K. (Ed.), Northern European Cenozoic Stratigraphy,  
1025 Proceedings of the 8th Biannual Meeting of the RPCSS/RNCSS. *Landesamt für Natur und Umwelt des Landes*  
1026 *Schleswig-Holstein, Flintbek*, 162–184.  
1027  
1028 Kasza, L. (1964). Geology of the upper basin of the Biala Łądecka stream. *Geol. Sudet*, 1, 119-167.

- 1029 Kontny, B. (2004). Is the Sudetic Marginal Fault still active? Results of the GPS monitoring 1996-2002. *Acta*  
1030 *Geodyn. Geomater.*, 1(135), 35-39.
- 1031
- 1032 Kroner, U., Mansy, J.-L., Mazur, S., Aleksandrowski, P., Hann, H.P., Huckriede, H., et al. (2008). Variscan  
1033 tectonics. In McCann, T. (Ed.), *The geology of Central Europe. The Geological Society, London*, pp. 599–664.  
1034 <http://doi.org/10.1144/CEVIP.11>
- 1035
- 1036 Krzyszkowski, D., & Pijet, E. (1993). Morphological effects of Pleistocene fault activity in the Sowie Mts.,  
1037 southwestern Poland. *Zeitschr. Geomorph., N. F., Suppl.-Bd. 94*, 243–259.
- 1038
- 1039 Krzyszkowski, D., Migoń, P., & Sroka, W. (1995). Neotectonic Quaternary history of the Sudetic Marginal fault,  
1040 SW Poland. *Folia Quaternaria*, 66, 73–98.
- 1041
- 1042 Krzyszkowski, D., Przybylski, B., & Badura, J. (2000). The role of neotectonics and glaciation on terrace formation  
1043 along the Nysa Kłodzka River in the Sudeten Mountains, southwestern Poland. *Geomorphology*, 33(3-4), 149–166.  
1044 [http://doi.org/10.1016/S0169-555X\(99\)00123-3](http://doi.org/10.1016/S0169-555X(99)00123-3)
- 1045
- 1046 Málek, J., Fischer, T., & Coubal, M. (1991). Computation of regional stress tensor from small scale tectonic data,  
1047 *Publ. Inst. Geophys. Pol. Acad. Sci., M-15(235)*, 77–92.
- 1048
- 1049 Malkovský, M. (1979). Tektogeneze platformního pokryvu Českého masívu (Tectogeny of the platform cover of the  
1050 Bohemian Massif). *Knihovna ÚÚG (Library of the Geological institute)*, 53, 176 pp. (in Czech)
- 1051
- 1052 Map portal of Czech Geological Survey. Last access: 14 Feb 2019. <https://mapy.geology.cz>
- 1053
- 1054 Marrett, R. A., & Allmendinger, R. W. (1990). Kinematic analysis of fault-slip data. *Journal of Structural Geology*,  
1055 12, 973-986. [http://doi.org/10.1016/0191-8141\(90\)90093-E](http://doi.org/10.1016/0191-8141(90)90093-E)
- 1056
- 1057 Mazur, S., Aleksandrowski, P., Kryza, R., & Oberc-Dziedzic, T. (2006). The Variscan Orogen in Poland. *Geol. Q.*,  
1058 50(1), 89–118.
- 1059
- 1060 Merle, O., & Michon, L. (2001). The formation of the West European rift. A new model as exemplified by the  
1061 Massif Central area. *Société Géologique de France*, 172, 213-221. <http://doi.org/10.2113/172.2.213>
- 1062
- 1063 Meulenkamp, J. E., Sissingh, W., Calvo, J. P., Daams, R., Londeix, L., Cahuzac, B., et al. (2000a). Late Tortonian  
1064 (8.4-7.2 Ma). In Dercourt J., Gaetani M., Vrielynck B., Barrier E., Biju-Duval B., Brunet F. M., et al. (Eds.): Peri-  
1065 Tethys Atlas, Palaeogeographic Maps with Explanatory Notes. *CCGM/CGMW, Paris*, 195-201.
- 1066
- 1067 Meulenkamp, J. E., Sissingh, W., Calvo, J. P., Daams, R., Londeix, L., Cahuzac, B., et al. (2000b). Piacenzian /  
1068 Gelasian (3.4-1.8 Ma). In Dercourt, J., Gaetani, M., Vrielynck, B., Barrier, E., Biju-Duval, B., Brunet, F. M., et al.  
1069 (Eds.): Peri-Tethys Atlas, Palaeogeographic Maps with Explanatory Notes. *CCGM/CGMW, Paris*, 203-208.
- 1070
- 1071 Morris, A., Ferrill, D. A., & Henderson, D.B. (1996). Slip tendency analysis and fault reactivation. *Geology* 24(3),  
1072 275-278. [http://doi.org/10.1130/0091-7613\(1996\)024<0275:STAAFR>2.3.CO;2](http://doi.org/10.1130/0091-7613(1996)024<0275:STAAFR>2.3.CO;2)
- 1073
- 1074 Müller, B., Zoback, M. L., Fuchs, K., Mastin, L., Gregersen, S., Pavoni, et al. (1992). Regional patterns of tectonic  
1075 stress in Europe. *J. geophys. Res.*, 97(B8), 11783-11803. <http://doi.org/10.1029/91JB01096>
- 1076
- 1077 Müller, V., & Čurda, J. (2003). Vysvětlivky k souboru geologických a ekologických účelových map přírodních  
1078 zdrojů v měřítku 1:50 000, Listy 04-43, 04-44, 14-21, 14-22, Bílý Potok, Javorník, Travná, Jeseník (Notes to  
1079 geological and ecological maps of nature resources in scale 1:50 000, Sheets 04-43, 04-44, 14-21, 14-22, Bílý Potok,  
1080 Javorník, Travná, Jeseník. *Czech Geological Survey*, 80 pp. (in Czech)
- 1081
- 1082 Nováková, L. (2010). Detail brittle tectonic analysis of the limestones in the quarries near Vápenná village (case  
1083 study). *Acta Geodyn. Geomater.*, 7(158), 167–174.



- 1084 Oberc, J. (1972). Budowa Geologiczna Polski, Tektonika, Sudety i obszary przyległe (Geological setting of the  
1085 Poland, Tectonics, Sudetes and surrounding area). *Wydawnictwa Geologiczne (Geological press), Warszawa*, 1–307.  
1086 (in Polish)  
1087
- 1088 Oberc, J., & Dyjor, S. (1969). Marginal Sudetic Fault. *Journal of the Geological Institute*, 236, 41-142. (in Polish  
1089 with English summary)  
1090
- 1091 Ondra P. (1968). Zpráva o vrtném průzkumu miocénní pánve u Uhelné ve Slezsku (Reports of the drilling campagne  
1092 within the Miocene graben by Uhelná village). *Geoscience Research Reports*, 1, 266-267. (in Czech)  
1093
- 1094 Osijuk, D., & Piwocki, M.: (1972). Osady spływów błotnych w utworach trzeciorzędowych okolic Ząbkowic  
1095 Śląskich (Run-off muds in the Tertiary formations near Ząbkowice Śląskie town). *Buil. Inst. Geol.*, 266, 110–125.  
1096 (in Polish)  
1097
- 1098 Pagaczewski, J. (1972). Catalogue of earthquakes in Poland in 1000–1970 years. *Mat. I*  
1099 *Prace Inst. Geofyz.*, 51, 36 pp.  
1100
- 1101 Peresson, H., & Decker, K. (1997a). Far-field effects of Late Miocene subduction in the Eastern Carpathians: E–W  
1102 compression and inversion of structures in the Alpine–Carpathian–Pannonian region. *Tectonics*, 16, 38–56.  
1103 <http://doi.org/10.1029/96TC02730>  
1104
- 1105 Peresson, H., & Decker, K. (1997b). The Tertiary dynamics of the Northern Eastern Alps (Austria): changing  
1106 paleostresses in a collisional plate boundary. *Tectonophysics*, 272, 125–157. [http://doi.org/10.1016/S0040-](http://doi.org/10.1016/S0040-1951(96)00255-7)  
1107 [1951\(96\)00255-7](http://doi.org/10.1016/S0040-1951(96)00255-7)  
1108
- 1109 Pešek, J. (Ed.) (1992). Terciární pánve a ložiska hnědého uhlí České republiky (Tertiary basins and deposits of  
1110 brown coal in Czech Republic). *Česká geologická služba (Czech geological survey)*, 438 pp. (in Czech)  
1111
- 1112 Peška, P. (1992). Stress indications in the Bohemian Massif: reinterpretation of borehole televiewer data. *Stud.*  
1113 *Geophys. Geod.*, 36(4), 307–324. <http://doi.org/10.1007/BF0162548>  
1114
- 1115 Pešková, I., Hók, J., Štěpančíková, P., Stemberk, J., & Vojtko, R. (2010). Results of stress analysis inferred from  
1116 fault slip data along the Sudetic Marginal Fault (NE part of Bohemian Massif). *Acta Geol. Slov.*, 2(1), 11-16.  
1117
- 1118 Piwocki, M., & Ziemińska-Tworzydło, M. (1995). Litostratygrafia i poziomy sporowo-pyłkowe neogenu na Niżu  
1119 Polskim (Neogene of the Polish Lowlands-lithostratigraphy and pollen-spore zones). *Prz. Geol.*, 43(1), 916–927.  
1120
- 1121 Piwocki, M., & Ziemińska-Tworzydło, M. (1997). Neogene of the Polish Lowlands – lithostratigraphy and pollen-  
1122 spore zones. *Geol. Quart.*, 41, 21–40.  
1123
- 1124 Pospíšil, L., Otava, J., & Hudečková, E. (2019). Utilization of archive geophysical data for geodynamical studies in  
1125 the Sudetes: Example of Bělá fault zone (The Nížký Jeseník Mts.). *Acta Geodyn. Geomater.*, 3(195), 281-291.  
1126 <https://doi.org/10.13168/AGG.2019.0024>  
1127
- 1128 Pouba, Z., & Misař, Z. (1961). O vlivu příčných zlomů na geologickou stavbu Hrubého Jeseníku (About the  
1129 influence of transversal faults to geological structure of the Hrubý Jeseník Mts.). *Journal for mineralogy and*  
1130 *geology*, IV. (in Czech)  
1131
- 1132 Przybylski, B., Badura, J., Czerwonka, J. A., Krzyszkowski, D., Krajewska, K., & Kuszell, T. (1998). Preglacial  
1133 Nysa Kłodzka fluvial system in the Sudetic Foreland, Southwestern Poland. *Geologia Sudetica*, 31, 171–196.  
1134
- 1135 Ramsay, J. G., & Huber, M. I. (1987). The Techniques of Modern Structure Geology, Volume 2: Folds and  
1136 Fractures. *Academic Press, London*, 309-697. <http://doi.org/10.1017/S0016756800010384>  
1137
- 1138 Ramsay, J. G., & Lisle, R. J. (2000). Modern Structure Geology, Volume 3: Applications of Continuum Mechanics  
1139 in Structure Geology. *Academic Press, London*, 1-560, [http://doi.org/10.1016/S0040-1951\(01\)00270-0](http://doi.org/10.1016/S0040-1951(01)00270-0)



- 1140  
1141 Rasser, M. V., & Harzhauser, M. (2008). Palaeogene and Neogene. In Mc Cann, T. (Ed.): The Geology of Central  
1142 Europe - Volume 2, Mesozoic and Cenozoic. *Geological Society, London*, 1031-1139.  
1143 <http://doi.org/10.1144/CEV2P.5>  
1144  
1145 Růžička, M. (2016). Geologie hydrogeologického rajonu 1621 Pliopleistocén Hornomoravského úvalu – sever  
1146 (Geology of the hydrogeological region 1621, Pliocene – Pleistocene in the northern part of the Upper Moravia  
1147 Graben). *Česká geologická služba (Czech geological survey), Geofond*, 18 pp. (in Czech)  
1148  
1149 Sawicki, L. (1997). Mapa geologiczna regionu Dolnośląskiego z przyległymi obszarami Czech i Niemiec 1:100 000,  
1150 Podstawy litostratygraficzne i kodyfikacja Wydzieleń (The geological map of the Lower Silesia with notes).  
1151 *Warszawa*, 181 pp. (in Polish)  
1152  
1153 Schenk, V., Cacoń, S., Bosy, J., Kontny, B., Kottnauer, P., & Schenková, Z. (2002). The GPS Geodynamic network  
1154 East Sudeten. Five annual campaigns (1997-2001), Data processing and results. *Acta Montana, A*, (124), 13-23.  
1155  
1156 Sissingh, W. (2001). Tectonostratigraphy of the West Alpine foreland: correlation of Tertiary sedimentary  
1157 sequences, changes in eustatic sea-level and stress regime. *Tectonophysics*, 233, 361–400.  
1158 [http://doi.org/10.1016/S0040-1951\(01\)00020-8](http://doi.org/10.1016/S0040-1951(01)00020-8)  
1159  
1160 Sissingh, W. (2003). Tertiary palaeogeographic and tectonostratigraphic evolution of the Rhenish Triple Junction.  
1161 *Palaeogeography, Palaeoclimatology, Palaeoecology*, 196, 229-263.  
1162 [http://doi.org/10.1016/S0031-0182\(03\)00320-1](http://doi.org/10.1016/S0031-0182(03)00320-1)  
1163  
1164 Sissingh, W. (2006). Syn-kinematic palaeogeographic evolution of the West European Platform: correlation with  
1165 Alpine plate collision and foreland deformation. *Neth. J. Geosci.*, 85, 131–180.  
1166 <http://doi.org/10.1017/S0016774600077933>  
1167  
1168 Skácel, J., & Vosyka, S. (1959). Přehled geologie Rychlebských hor (Geology of the Rychlebské hory Mts.).  
1169 *Rychlebské hory - sborník prací o přírodních poměrech (Rychlebské hory Mts. proceedings)*, 30, 9-45. (in Czech)  
1170  
1171 Skácel, J. (1963). Geologie krystalinika a rudních výskytů ve střední části Rychlebských hor (Geology of the  
1172 crystalline complex and ore in central part of the Rychlebské hory Mts). *Journal of Geological Sciences*, 3, 109-139.  
1173 (in Czech)  
1174  
1175 Skácel, J. (1989). Křížení okrajového zlomu lugičana a nýznerovského dislokačního pásma mezi Vápennou a  
1176 Javorníkem ve Slezsku. (Crossing of the Lugičana marginal fault and Nýznerov dislocation zone between Vápenná  
1177 and Javorník). *Acta Univer. Palackianae Olomucensis. Facultas rerum naturalium, T. 29. Geogr.-Geol.* 28(95), 31-  
1178 45. (in Czech)  
1179  
1180 Skácel, J. (2004). The Sudetic Marginal Fault between Bílá Voda and Lipová Lázně. *Acta Geodyn. Geomater.*,  
1181 1(145), 31-33.  
1182  
1183 Skácelová, D. (Ed.) (1992a). Geologická mapa ČR, 1:50 000, list 04-43 Bílý Potok (Geological map of the Czechia  
1184 in scale 1:50 000, sheet 04-43 Bílý Potok. *Czech Geological Institute*.  
1185  
1186 Skácelová, D. (Ed.) (1992b). Geologická mapa ČR, 1:50 000, list 14-21 Travná (Geological map of the Czechia in  
1187 scale 1:50 000, sheet 14-21 Travná. *Czech Geological Institute*.  
1188  
1189 Skácelová, D. (Ed.) (1997). Geologická mapa ČR, 1:50 000, list 04-44 Javorník (Geological map of the Czechia in  
1190 scale 1:50 000, sheet 04-44 Javorník. *Czech Geological Institute*.  
1191  
1192 Sperner, B., & Zweigel, P. (2010). A plea for more caution in fault-slip analysis. *Tectonophysics*, 482(1–4), 29-41.  
1193 <http://doi.org/10.1016/j.tecto.2009.07.019>  
1194

- 1195 Špičáková, L., Uličný, D., & Koudelková, G. (2000). Tectonosedimentary evolution of the Cheb Basin (NW  
1196 Bohemia, Czech Republic) between Late Oligocene and Pliocene: a preliminary note. *Studia geoph. et geod.*, 44(4),  
1197 556-580. <http://doi.org/10.1023/A:1021819802569>  
1198
- 1199 Stemberk, J., Jr., Coubal, M., Stemberk, J., & Štěpančíková, P. (2019). Stress analysis of slips data recorded within  
1200 the Dědičná štola Gallery in the Rychlebské hory Mts., NE part of the Bohemian Massif. *Acta Geodyn. Geomater.*,  
1201 16(195), 315-330. <http://doi.org/10.13168/AGG.2019.0027>  
1202
- 1203 Stemberk, J., Jr. (2020). Striae on slickensides within the Lutynia/Ladek Zdroj area for SW Faultkin7 and  
1204 ROCK2014. *Mendeley Data*, v1. <http://dx.doi.org/10.17632/p98hwk5mwn.1>  
1205
- 1206 Špaček, P., Sýkorová, Z., Pazdírková, J., Švancara, J., & Havíř, J. (2006). Present-day seismicity of the south-  
1207 eastern Elbe Fault System (NE Bohemian Massif). *Studia Geophysica et Geodaetica*, 50(2), 233-258.  
1208 <http://doi.org/10.1007/s11200-006-0014-z>  
1209
- 1210 Špaček, P., Bábek, O., Štěpančíková, P., Švancara, J., Pazdírková, J., & Sedláček, J. (2015). The Nysa-Morava  
1211 Zone: an active tectonic domain with Late Cenozoic sedimentary grabens in the Western Carpathians' foreland (NE  
1212 Bohemian Massif). *International journal of earthquakes*, 104(4), 963-990. [http://doi.org/10.1007/s00531-014-1121-](http://doi.org/10.1007/s00531-014-1121-7)  
1213 [7](http://doi.org/10.1007/s00531-014-1121-7)  
1214
- 1215 Štěpančíková, P., Stemberk, J., Vilímecký, V., & Košťák, B. (2008). Neotectonic development of drainage networks in  
1216 the East Sudeten Mountains and monitoring of recent fault displacements (Czech Republic). *Geomorphology*, 102,  
1217 68-80. <http://doi.org/10.1016/j.geomorph.2007.06.016>  
1218
- 1219 Štěpančíková, P., Hók, J., Nývlt, D., Dohnal, J., Sýkorová, I., & Stemberk, J. (2010). Active tectonics research using  
1220 trenching technique on the south-eastern section of the Sudetic Marginal Fault (NE Bohemian Massif, central  
1221 Europe). *Tectonophysics*, 485(1-4), 269-282. <http://doi.org/10.1016/j.tecto.2010.01.004>  
1222
- 1223 Štěpančíková, P., & Stemberk, J. Jr. (2016). Region of the Rychlebské Hory Mountains - Tectonically Controlled  
1224 Landforms and Unique Landscape of Granite Inselbergs (Sudetic Mountains). In Migoń, P., Landscape and  
1225 landforms of the Czech Republic, Book Series: World Geomorphological Landscapes. *Springer*, 263-276.  
1226 [http://doi.org/10.1007/978-3-319-27537-6\\_21](http://doi.org/10.1007/978-3-319-27537-6_21)  
1227
- 1228 Ulrych, J., Ackerman, L., Balogh, K., Hegner, E., Jelínek, E., Pécskay, et al. (2013). Plio-Pleistocene basaltic and  
1229 mellitic series of the Bohemian Massif: K-Ar ages, major/trace element and Sr-Nd isotopic data. *Chemie der Erde*,  
1230 73, 429-450. <http://doi.org/10.1016/j.chemer.2013.02.001>  
1231
- 1232 Ustaszewski, K., & Schmid, S. M. (2006). Control of preexisting faults on geometry and kinematics in the  
1233 northernmost part of the Jura fold-and-thrust belt. *Tectonics*, 25, TC5003, 1-26.  
1234 <http://doi.org/10.1029/2005TC001915>.  
1235
- 1236 Vavryčuk, V., Bouchaala, F., & Fischer, T. (2013). High-resolution fault image from accurate locations and focal  
1237 mechanisms of the 2008 swarm earthquakes in West Bohemia, Czech Republic. *Tectonophysics*, 590, 189-195.  
1238 <http://doi.org/10.1016/j.tecto.2013.01.025>  
1239
- 1240 Walczak, W. (1954). Pradolina Nysy i plejstocenske zmiany hydrograficzne na przedpolu Sudetow Wschodnich  
1241 (The paleovalley of Nysa river and hydrographic changes in Eastern Foresudetic area during Pleistocene). *Polska*  
1242 *Akademia Nauk, Instytut Geografii (Polish Academy of Sciences, Institute of Geography), Prace Geograficzne*  
1243 *(Journal of Geology)*, 2, 51 pp. (in Polish)  
1244
- 1245 Walczak, W. (1970) Obszar przedsudecki. Dolny Śląsk. Cz. II – Obszar przedsudecki (The Fore-Sudetic area,  
1246 Lower Silesia). *Państwowe wydawnictwo naukowe, Warszawa*, 415 pp. (in Polish)  
1247
- 1248 Zedník, J., Pospíšil, J., Růžek, B., Horálek, J., Boušková, A., & Jedlička, P. (2001). Earthquakes in the Czech  
1249 Republic and surrounding regions in 1995-1999. *Stud. Geophys. et Geod.*, 45, 267-282.  
1250 <http://doi.org/10.1023/A:1022084112758>

- 1251  
1252 Ziegler, P. A. (1992). European Cenozoic rift system. In Ziegler, P. A. (Ed.), *Geodynamics of Rifting, Volume I.*  
1253 *Case History Studies on Rifts: Europe and Asia. Tectonophysics*, 208, 91-111. [http://doi.org/10.1016/0040-](http://doi.org/10.1016/0040-1951(92)90338-7)  
1254 [1951\(92\)90338-7](http://doi.org/10.1016/0040-1951(92)90338-7)  
1255  
1256 Ziegler, P. A., & Dèzes, P. (2007). Cenozoic uplift of Variscan Massifs in the Alpine foreland: Timing and  
1257 controlling mechanisms. *Global and Planetary Change* 58, 237-269. <http://doi.org/10.1016/j.gloplacha.2006.12.004>